IMMUNOLOGY

Isocyanic acid–mediated NLRP3 carbamoylation reduces NLRP3-NEK7 interaction and limits inflammasome activation

Zhenxing Zhang[1]†, Chao Chen[1]†, Caiyun Liu[1,2], Pengkai Sun[1,2], Ping Liu[1], Shu Fang[1,2], Xinjian Li[1,2]*

Isocyanic acid, as a reactive metabolite synthesized by the enzyme LACC1, can carbamoylate the ε-amino group of lysine residues in proteins. However, the role of isocyanic acid in inflammatory response remains elusive. Herein, we reveal that lipopolysaccharide stimulation increases LACC1-dependent isocyanic acid production, which attenuates inflammation by limiting the NLRP3 inflammasome activation in macrophages primed with lipopolysaccharide for 8 hours. Mechanistically, isocyanic acid directly carbamoylates NLRP3 at lysine-593 to disrupt NLRP3-NEK7 interaction, a key step in assembly of active NLRP3 inflammasome. Abrogation of isocyanic acid biosynthesis by *LACC1*/*Lacc1* knockout or expression of K593 carbamoylation (K593ca)–deficient NLRP3 mutant promotes macrophagic inflammatory response in vitro. Furthermore, *Lacc1*$^{-/-}$ mice and mice harboring K593ca-deficient NLRP3 mutation manifest exacerbated inflammatory response in vivo. Hence, our findings identify isocyanic acid as an endogenous immunoregulatory metabolite that limits NLRP3-driven inflammation and provide valuable insights into the regulation of NLRP3 inflammasome activation, governed by metabolites.

INTRODUCTION

Inflammasomes function as important innate immune sensors that are activated in response to microbial invasion and damage signals (*1*, *2*). Numerous different types of inflammasomes and their corresponding activating stimuli have been identified. Among inflammasomes, the nucleotide-binding oligomerization domain (NOD)–, leucine-rich repeat (LRR)–, and pyrin domain (PYD)–containing protein 3 (NLRP3) inflammasome, consisting of the central protein NLRP3, the adaptor protein apoptosis-associated speck-like protein containing a caspase-recruitment domain (CARD) (ASC, also known as PYCARD), the mitotic kinase never in mitosis gene a (NIMA)–related kinase 7 (NEK7), and the effector protein caspase-1, has been studied extensively and was found to be activated by a wide spectrum of stimuli (*3*). Structurally, NLRP3 can be divided into three domains: an N-terminal PYD, a C-terminal LRR domain, and a central NACHT [an acronym standing for neuronal apoptosis inhibitory protein (NAIP), major histocompatibility complex class II transcription activator (CIITA), incompatibility locus protein from *Podospora anserina* (HET-E), and telomerase-associated protein 1 (TP1)] domain (*4*). The LRR and NACHT domains interacting with NEK7 are essential for the NLRP3 inflammasome complex assembly (*4*). Activation of the NLRP3 inflammasome triggers autocatalytic activation of caspase-1 (CASP1), leading to processing the proinflammatory cytokines interleukin-1β (IL-1β) and IL-18 for their maturation, and cleaving gasdermin D (GSDMD) to induce pyroptosis (*5*, *6*). Following the GSDMD cleavage, NINJ1, a 16-kDa plasma membrane protein that is evolutionarily conserved and found in all higher eukaryotes, induces plasma membrane rupture (PMR), which is the final cataclysmic event in lytic cell death (*7*–*10*). It is known that aberrant activation of NLRP3 inflammasome is the etiology of a series of inflammatory, autoimmune, and degenerative diseases (*3*); thus, a better understanding of the molecular mechanisms underlying NLRP3 inflammasome activation remains necessary.

Numerous studies have shown that macrophages may undergo metabolic reprogramming in response to pathogen invasion. Laccase domain containing 1 (LACC1), also known as chromosome 13 open reading frame 31 (C13orf31) or fatty acid metabolism-immunity nexus (FAMIN), is a metabolic enzyme highly expressed in inflammatory macrophages and serves as a central regulator for immune-metabolic function in classically activated macrophages (*11*–*14*). LACC1 is also a multifunctional purine nucleoside enzyme participating in several purine nucleotide metabolic reactions (*15*, *16*). In addition, LACC1 may act as an isocyanic acid synthase that catalyzes the cleavage of citrulline into ornithine and isocyanic acid (*17*). Notably, as tautomer, isocyanic acid and cyanate can interconvert each other (*18*). Owing to its highly reactive property, isocyanic acid could react with the ε-amino group of a lysine residue to form a homocitrulline residue in target proteins, which is also referred as carbamoylation (*18*). It has been known that isocyanic acid–mediated protein carbamoylation is associated with the development of renal and cardiovascular disease (*19*–*22*). However, it is still unknown whether isocyanic acid serves as an immune effector.

Here, we demonstrate that isocyanic acid produced by LACC1 directly carbamoylates NLRP3 at lysine-593 and limits NLRP3 inflammasome activation by disrupting the interaction between NLRP3 and NEK7 in inflammatory macrophages. In addition, *Lacc1*$^{-/-}$ mice and *Nlrp3* K593R mice exhibit exacerbated inflammatory response in the inflammation models established by injection of lipopolysaccharide (LPS) or monosodium urate (MSU) crystals in vivo. Isocyanic acid may thereby be a negative regulator of NLRP3 inflammasome, which could provide valuable insights into the regulation of NLRP3 inflammasome activation, governed by metabolites.

[1]State Key Laboratory of Epigenetic Regulation and Intervention, Institute of Biophysics, Chinese Academy of Sciences, Beijing 100101, China. [2]College of Life Sciences, University of Chinese Academy of Sciences, Beijing 100049, China.
*Corresponding author. Email: lixinjian@ibp.ac.cn
†These authors contributed equally to this work.

RESULTS

LACC1 limits NLRP3 inflammasome activation

Isocyanic acid synthase LACC1 is robustly activated by LPS in murine bone marrow–derived macrophages (mBMDMs) (*11*, *12*, *17*). Consistent with the previous studies, full induction of LACC1 expression was observed in THP-1 cells and immortalized BMDMs (iBMDMs) stimulated with LPS for 8 hours (fig. S1A). Next, to determine whether LACC1 is involved in the activation of NLRP3 inflammasome, we knocked out *LACC1*/*Lacc1* in THP-1 cells and iBMDMs. As expected, loss of LACC1 expression was observed in *LACC1*/*Lacc1*-knockout (KO) THP-1 cells and iBMDMs stimulated with LPS for 8 hours, as detected by immunoblotting analysis (Fig. 1A). Enzyme-linked immunosorbent assay (ELISA) revealed that *LACC1*/*Lacc1* KO increased the releases of IL-1β (Fig. 1B), IL-18 (Fig. 1C), and lactate dehydrogenase

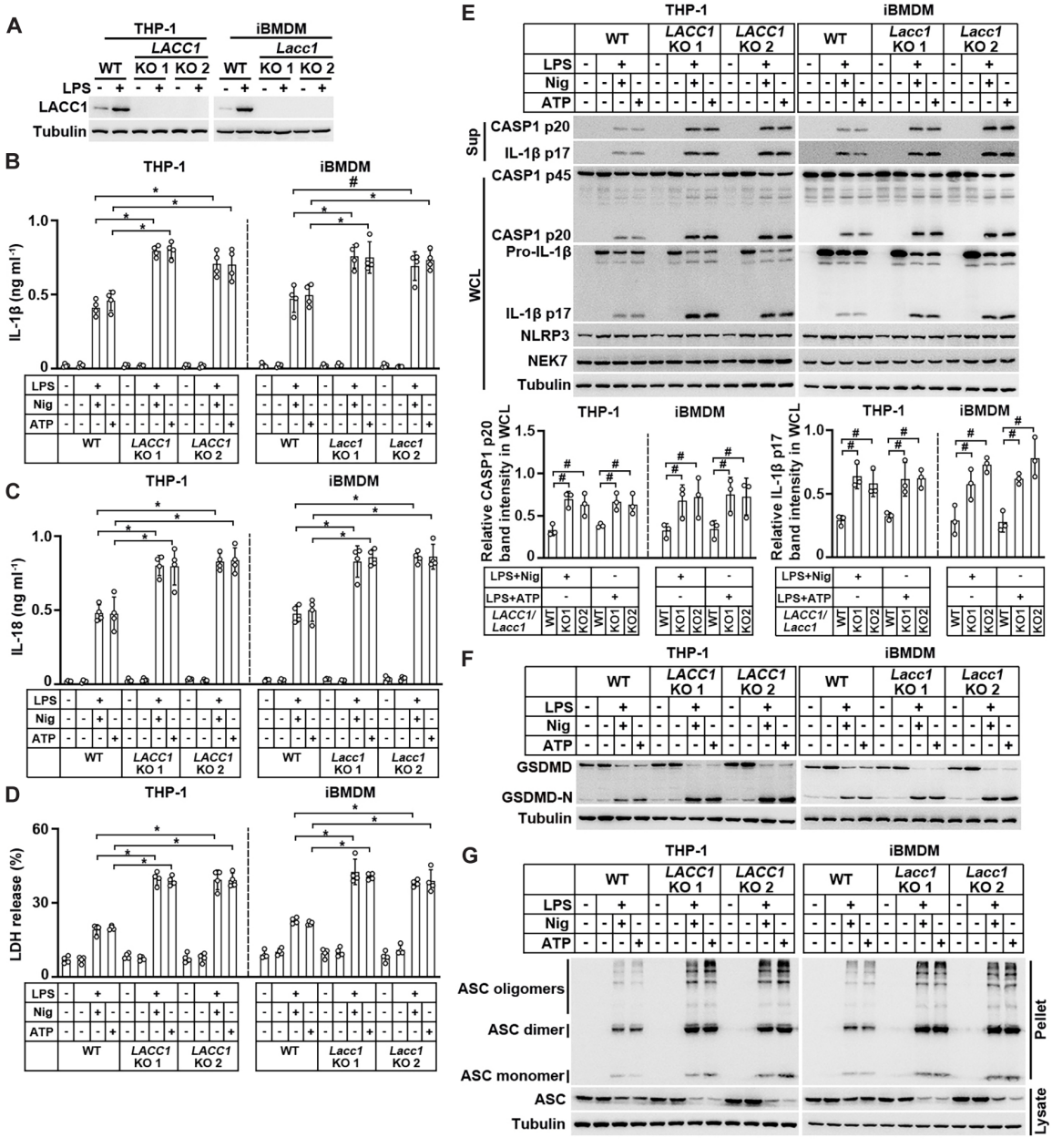

Fig. 1. LACC1 limits NLRP3 inflammasome activation. PMA-differentiated THP-1 cells and iBMDMs without or with *LACC1*/*Lacc1* KO were stimulated with LPS (100 ng ml^{-1}) for 8 hours (**A**) and then incubated with 10 μM Nig or 5 mM ATP for another 45 min (**B** to **G**). *P* values were calculated using one-way ANOVA (B to E). The data are presented as mean ± SD of three (E) or four (B to D) independent experiments. $^{*}P < 0.01$, $^{\#}P < 0.05$. (A) LACC1 in the lysates of indicated cells was analyzed by immunoblotting. (B to D) The release of IL-1β (B), IL-18 (C), and LDH (D) in culture supernatants was determined by ELISA. (E) Pro- and mature caspase-1 and IL-1β, NLRP3, and NEK7 proteins in whole-cell lysates (WCL), and CASP1 p20 and IL-1β p17 in culture supernatants (Sup) were analyzed by immunoblotting (top). Band intensity of mature caspase-1 (CASP1 p20) and IL-1β (IL-1β p17) in the WCL with normalization to tubulin was shown (bottom). (F) Cleavage of GSDMD was analyzed by immunoblotting. (G) The formation of large multimeric ASC complexes was analyzed by immunoblotting.

(LDH) (Fig. 1D) upon NLRP3 inflammasome activation using nigericin (Nig) or adenosine triphosphate (ATP) in LPS-primed THP-1 cells and iBMDMs. By contrast, *LACC1*/*Lacc1* KO did not alter the LPS-induced secretion of tumor necrosis factor–α (TNF-α) in THP-1 cells and iBMDMs (fig. S1B). Consistently, immunoblotting analysis demonstrated that *LACC1*/*Lacc1* KO promoted the LPS-Nig/ATP–induced cleavages of IL-1β and caspase-1 to their mature subunits, which are p17 and p20, but did not alter the expression levels of NLRP3 and NEK7 in THP-1 cells and iBMDMs (Fig. 1E). Moreover, *LACC1*/*Lacc1* KO promoted the LPS-Nig/ATP–induced formation of the active N-terminal fragment of GSDMD (GSDMD-N) (Fig. 1F) and the large multimeric ASC complexes (Fig. 1G) in these cells. Additionally, quantitative polymerase chain reaction (qPCR) analysis indicated that wild-type (WT) and *LACC1*/*Lacc1*-KO THP-1 cells and iBMDMs displayed similar mRNA levels of NLRP3 inflammasome components, including *NLRP3*/*Nlrp3*, *NEK7*/*Nek7*, *ASC*/*Asc*, *CASP1*/*Casp1*, *IL-1B*/*Il-1b*, *IL-18*/*Il-18*, *GSDMD*/*Gsdmd*, and *NINJ1*/*Ninj1*, upon LPS stimulation (fig. S1C), suggesting that LACC1 is not required for the expression of NLRP3 inflammasome components in LPS-stimulated macrophages. Together, these results support that LACC1 limits NLRP3 inflammasome activation in macrophages.

Previous study demonstrates that inhibitor of nuclear factor κB kinase subunit β (IKKβ)–mediated NEK7-independent pathway constitutes the predominant NLRP3 priming mechanism in human myeloid cells (*23*). To test whether LACC1 regulated NLRP3 inflammasome activity in a NEK7-dependent manner in human macrophages, we knocked out *LACC1* in WT, *NEK7*-KO, or *IKBKB* (the gene coding for IKKβ)–KO THP-1 cells. As expected, loss of NEK7, IKKβ, and/or LACC1 expression was observed in these cells, as detected by immunoblotting analysis (fig. S1D). Consistent with the previous study (*23*), *NEK7* KO or *IKBKB* KO partially inhibited the LPS-Nig–induced releases of IL-1β (fig. S1E), IL-18 (fig. S1F), and LDH (fig. S1G) in THP-1 cells. However, *LACC1* KO increased the LPS-Nig–induced releases of IL-1β (fig. S1E), IL-18 (fig. S1F), and LDH (fig. S1G) in WT and *IKBKB*-KO, but not *NEK7*-KO, THP-1 cells. These data support that LACC1 limits NLRP3 inflammasome activation depending on NEK7, but not IKKβ, in human macrophages.

To investigate whether LACC1 exerts its immunoregulatory function depending on the inflammasomes other than NLRP3 inflammasome, we tested the effect of *LACC1*/*Lacc1* KO on activation of AIM2 and NLRC4 inflammasome. Notably, *LACC1*/*Lacc1* KO did not alter the releases of IL-1β (fig. S1H) and LDH (fig. S1I), the cleavages of IL-1β and caspase-1 (fig. S1J), and the GSDMD-N formation (fig. S1K) when the AIM2 inflammasome was activated with poly(deoxyadenylic-deoxythymidylic) [poly(dA:dT)] transfection in LPS-primed THP-1 cells and iBMDMs. Similar effects were observed when the NLRC4 inflammasome was activated with flagellin transfection in LPS-primed THP-1 cells and iBMDMs (fig. S1, L to O). Next, we tested the effect of *LACC1*/*Lacc1* KO on noncanonical inflammasome signaling, in that cytosolic LPS–activated caspase-11 (caspase-4 and caspase-5 in humans) cleaves GSDMD to induce pyroptosis, and then canonical activation of NLRP3 inflammasome resulting from pyroptosis-mediated K^+ efflux triggers the release of IL-1β (*24*). We observed that *LACC1*/*Lacc1* KO increased IL-1β release (fig. S1P), but not pyroptosis, as measured by the release of LDH (fig. S1Q) when the noncanonical inflammasome was activated with LPS transfection in LPS-primed THP-1 cells and iBMDMs. Collectively, these data support that LACC1 limits canonical and noncanonical activation of NLRP3 inflammasome, but not AIM2 and NLRC4 inflammasome.

Isocyanic acid produced by LACC1 limits NLRP3 inflammasome activation

It has been reported that LACC1 is an enzyme converting citrulline into isocyanic acid and ornithine (*17*). Liquid chromatography–mass spectrometry (LC-MS) analysis revealed that LPS stimulation dramatically increased intracellular levels of isocyanic acid in WT, but not *LACC1*/*Lacc1*-KO, THP-1 cells and iBMDMs (Fig. 2A). Likewise, a moderate increase in intracellular levels of ornithine was observed in WT, but not *LACC1*/*Lacc1*-KO, THP-1 cells and iBMDMs upon LPS stimulation (fig. S2A). Next, to further examine the role of LACC1 in the route of isocyanic acid production in inflammatory macrophages, WT and *LACC1*/*Lacc1*-KO THP-1 cells and iBMDMs were stimulated with LPS for 8 hours in the presence of ureido-^{13}C–labeled citrulline in the culture medium. As expected, *LACC1*/*Lacc1* KO abrogated ^{13}C-isocyanic acid production in these cells upon LPS stimulation (fig. S2B). Together, these data support that LACC1 produces isocyanic acid from citrulline in inflammatory macrophages.

Furthermore, to determine whether citrulline is required for isocyanic acid production in inflammatory macrophages, THP-1 cells and iBMDMs were infected with the control lentiviruses expressing green fluorescent protein (GFP) or the lentiviruses expressing argininosuccinate synthetase-1 (ASS1), an enzyme converting citrulline to argininosuccinate (*25*), under the control of a doxycycline-inducible promoter. Following the doxycycline treatment, a depletion of intracellular citrulline was observed in THP-1 cells and iBMDMs ectopically expressing ASS1 (fig. S2, C and D). LPS stimulation increased intracellular isocyanic acid levels in GFP-expressed THP-1 cells and iBMDMs (fig. S2E); however, this effect was abrogated by ectopic expression of ASS1 in THP-1 cells and iBMDMs (fig. S2E). These data support that citrulline is required for isocyanic acid production in inflammatory macrophages.

Given the observation that LACC1 loss promoted NLRP3 inflammasome activation and LACC1 produces isocyanic acid in LPS-stimulated macrophages, we hypothesized that LACC1-synthesized isocyanic acid limits NLRP3 inflammasome activation in inflammatory macrophages. To test this hypothesis, we infected the WT and *LACC1*/*Lacc1*-KO THP-1 cells and iBMDMs with the control lentiviruses expressing GFP or the lentiviruses expressing cyanase, an enzyme degrading isocyanic acid (*26*), under the control of a doxycycline-inducible promoter. Following the doxycycline treatment, we found that *LACC1*/*Lacc1*-KO THP-1 cells and iBMDMs exposed to 1 mM exogenous cyanate, a tautomer of isocyanic acid that may interconvert with cyanate (*18*), displayed an intracellular isocyanic acid level similar to that of LPS-stimulated WT cells expressing GFP (fig. S2, F and G). Strikingly, intracellular isocyanic acid was undetectable when cyanase was expressed in these cells (fig. S2, F and G), suggesting that our detection of intracellular isocyanic acid is reliable. Accordingly, exogenous cyanate (1 mM) abolished the exacerbated NLRP3 inflammasome activation resulting from *LACC1*/*Lacc1* KO, as evidenced by the observations that *LACC1*/*Lacc1* KO–promoted releases of IL-1β (Fig. 2B), IL-18 (Fig. 2C), and LDH (Fig. 2D); cleavages of IL-1β and caspase-1 to their active forms (Fig. 2E); formation of GSDMD-N (Fig. 2F); and large multimeric ASC complexes (Fig. 2G) were abrogated by pretreating these cells with 1 mM cyanate before NLRP3 inflammasome activation, although *LACC1*/*Lacc1* KO did not alter the expression levels of NLRP3 and NEK7 in these cells (Fig. 2E). By contrast, similar effects on NLRP3 inflammasome activation were not observed when these cells were pretreated with the same concentrations of ornithine (fig. S3, A to

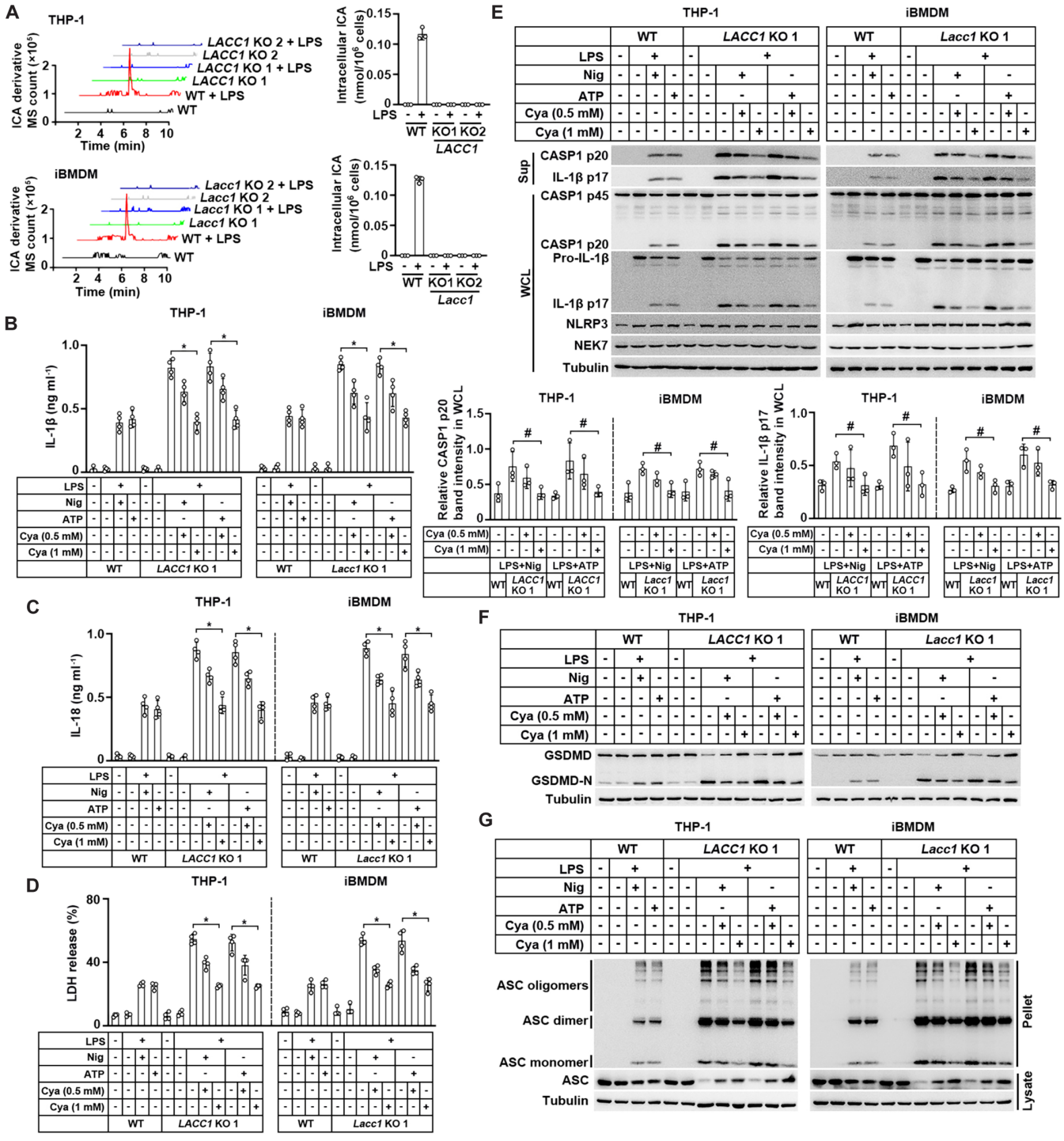

Fig. 2. LACC1-produced isocyanic acid limits NLRP3 inflammasome activation. (**A** to **G**) THP-1 cells and iBMDMs without or with *LACC1*/*Lacc1* KO were stimulated with LPS (100 ng ml^{-1}) for 8 hours. (B to G) The LPS-primed macrophages were pretreated without or with indicated concentrations (0.5 and 1 mM) of cyanate (Cya) for 30 min and then incubated with 10 μM Nig or 5 mM ATP for another 45 min. (A) Intracellular levels of isocyanic acid (ICA) were detected by LC-MS analysis. (B to D) The release of IL-1β (B), IL-18 (C), and LDH (D) in culture supernatants was determined by ELISA. (E) Pro- and mature caspase-1 and IL-1β, NLRP3, and NEK7 proteins in WCL, and CASP1 p20 and IL-1β p17 in culture supernatants were analyzed by immunoblotting (top). Band intensity of mature caspase-1 (CASP1 p20) and IL-1β (IL-1β p17) in the WCL with normalization to tubulin was shown (bottom). (F) Cleavage of GSDMD was analyzed by immunoblotting. (G) The formation of large multimeric ASC complexes was analyzed by immunoblotting. The data are presented as mean ± SD of three (A and E) or four (B to D) independent experiments. *P* values were calculated using one-way ANOVA (B to E). $^{*}P < 0.01$, $^{\#}P < 0.05$.

F). Together, these data suggest that LACC1-synthesized isocyanic acid limits NLRP3 inflammasome activation in inflammatory macrophages.

Furthermore, to investigate the effect of exogenous cyanate treatment on NLRP3 inflammasome activation in *LACC1*/*Lacc1*-competent macrophages, we treated the LPS-primed WT THP-1 cells and iBMDMs with 1 mM cyanate before NLRP3 inflammasome activation and found that cyanate did not alter the releases of IL-1β (fig. S4A), IL-18 (fig. S4B), and LDH (fig. S4C); cleavages of IL-1β and caspase-1 to their active forms (fig. S4D); formation of GSDMD-N (fig. S4E); and appearance of large multimeric ASC complexes (fig. S4F) in these cells, supporting that exogenous cyanate treatment cannot exert detectable impacts on NLRP3 inflammasome activation in *LACC1*/*Lacc1*-competent macrophages.

Next, to test the toxicity of isocyanic acid toward macrophages, WT and *LACC1*/*Lacc1*-KO THP-1 cells and iBMDMs were treated with exogenous cyanate. As expected, treatment with exogenous cyanate (0.5 or 1 mM) did not exert significant impact on the viability of WT and *LACC1*/*Lacc1*-KO THP-1 cells and iBMDMs (fig. S4G), suggesting that treatment with exogenous cyanate at a concentration no more than 1 mM is not toxic for macrophages.

LACC1 produces isocyanic acid in a urea- and MPO-independent manner

It has been reported that isocyanic acid is formed via the decomposition of urea or myeloperoxidase (MPO)–catalyzed oxidation of thiocyanate (*19*, *21*). To examine the effect of urea on LACC1-dependent isocyanic acid production in macrophages, WT and *LACC1*/*Lacc1*-KO THP-1 cells and iBMDMs were infected with the control lentiviruses expressing GFP or the lentiviruses expressing urease, an enzyme hydrolyzing urea (*27*), under the control of a doxycycline-inducible promoter. Following the doxycycline treatment, intracellular urea was detected in GFP-expressed, but not urease-expressed, THP-1 cells and iBMDMs without or with LPS stimulation (fig. S5, A and B). Strikingly, urease expression (fig. S5A) did not alter the LACC1-dependent isocyanic acid production (fig. S5C) in THP-1 cells and iBMDMs upon LPS stimulation. These data suggest that LACC1 produces isocyanic acid in a urea-independent manner in LPS-stimulated macrophages. Moreover, immunoblotting analysis revealed that MPO expression was undetectable in THP-1 cells and iBMDMs without or with LPS stimulation (fig. S5D), implying that MPO is also not involved in LACC1-dependent isocyanic acid production in inflammatory macrophages.

Isocyanic acid carbamoylates NLRP3 at K593 to disrupt the interaction between NLRP3 and NEK7

Given that isocyanic acid could potentially carbamoylate protein lysine residues by a nonenzymatic reaction and ASC and caspase-1 are components shared by other inflammasomes, we subsequently hypothesized that the acute and specific effect of isocyanic acid on NLRP3 activation may result from carbamoylation of NLRP3 and/or NEK7 directly. NLRP3 and NEK7 interact with each other upon NLRP3 inflammasome activation (*4*). To test whether isocyanic acid–mediated carbamoylation affects the interaction between NLRP3 and NEK7 upon NLRP3 inflammasome activation, we reconstituted a murine NLRP3 inflammasome in 293T cells stably expressing the pore-forming protein GSDMD (*28*, *29*). As expected, immunoprecipitation analysis revealed that treatment with exogenous cyanate before Nig stimulation disrupted the interaction between NLRP3 and NEK7 in 293T cells expressing GSDMD and the reconstituted murine NLRP3 inflammasome (Fig. 3A). Consistently, exogenous cyanate blocked the release of CASP1 p20, the active form of caspase-1, from 293T cells upon Nig stimulation (Fig. 3A). Subsequent MS/MS of murine NLRP3, immunoprecipitated from ^{15}N-labeled cyanate-treated FLAG-tagged NLRP3-overexpressing iBMDMs, showed that cyanate carbamoylated (+44.013 Da) multiple lysine residues on NLRP3 (Fig. 3, B and C, and fig. S6A). To determine the carbamoylation site disrupting the interaction between NLRP3 and NEK7, we mutated the carbamoylated lysine (K) residues, which are identified by MS/MS analysis, to arginine (R) in NLRP3 protein and utilized these proteins to reconstitute a murine NLRP3 inflammasome (*29*). Immunoprecipitation analysis revealed that NLRP3 K593R mutation abrogated the cyanate-mediated disruption of interaction between NLRP3 and NEK7 (Fig. 3D), suggesting that NLRP3 K593 carbamoylation (K593ca) is required to disrupt the interaction between NLRP3 and NEK7 upon NLRP3 inflammasome activation.

It has been reported that the pathogenic LACC1 mutations, including T276fs*2 (*30*) and A278P (*31*), are causal for a monogenic form of juvenile idiopathic arthritis (JIA). To test the effect of pathogenic LACC1 mutations on NLRP3 inflammasome activation, we reconstituted murine NLRP3 inflammasome in 293T cells stably expressing GSDMD. Upon NLRP3 inflammasome activation, expression of WT LACC1, but not the LACC1 T276fs*2 and A278P, significantly increased NLRP3 K593ca and blocked the cleavages of caspase-1 and GSDMD to their active forms (fig. S6B). Consistently, LC-MS analysis revealed that expression of WT LACC1, but not the LACC1 T276fs*2 and A278P, dramatically increased intracellular levels of isocyanic acid in these cells (fig. S6C). These data support that LACC1 mutations may be causal for the exacerbated NLRP3 inflammasome activation during JIA progress.

We next performed an in vitro carbamoylation assay by incubating cyanate with purified recombinant WT NLRP3 or NLRP3 K593R protein (amino acid 139 to 1033 truncation) fused with His-MBP (maltose binding protein) tag at the N terminus (fig. S6D). As expected, K593ca on WT NLRP3, but not NLRP3 K593R, was detected by a custom-designed and specificity-validated anti–NLRP3 K593ca antibody (Fig. 4A and fig. S6E). Furthermore, glutathione *S*-transferase (GST) pull-down assay demonstrated that cyanate incubation blocked the binding of WT NLRP3, but not NLRP3 K593R, to purified GST-tagged NEK7 (Fig. 4B and fig. S6D). In line with these in vitro results, LPS stimulation dramatically increased NLRP3 K593ca in WT, but not *LACC1*/*Lacc1*-KO, THP-1 cells and iBMDMs (Fig. 4C); however, cyanate treatment recovered the NLRP3 K593ca in *LACC1*/*Lacc1*-KO THP-1 cells and iBMDMs stimulated with LPS (Fig. 4C). Stoichiometry analysis demonstrated that K593-carbamoylated NLRP3 accounted for about 80% of total NLRP3 in THP-1 cells and iBMDMs (fig. S6F). Moreover, previous studies reported that the majority of NLRP3 protein is localized in cytosol (*32*). To examine whether LACC1 is colocalized with NLRP3, extracts from THP-1 cells and iBMDMs were fractionated into P5 (heavy membrane), P100 (light membrane), and S100 (cytosol) fractions by differential centrifugation. Immunoblotting analysis indicated that LACC1 is colocalized with NLRP3 in S100 fraction (fig. S6G), suggesting that isocyanic acid generated by LACC1 may carbamoylate NLRP3 in cytosol. Additionally, immunoprecipitation analysis indicated that *LACC1*/*Lacc1* KO increased the LPS-Nig/ATP–induced interaction between NLRP3 and NEK7 and this effect was abrogated by cyanate treatment (Fig. 4D).

Next, to further validate our findings in THP-1 cells and iBMDMs, we knocked out endogenous *NLRP3*/*Nlrp3* and reconstitutively expressed the counterpart FLAG-tagged WT guide RNA (gRNA)–

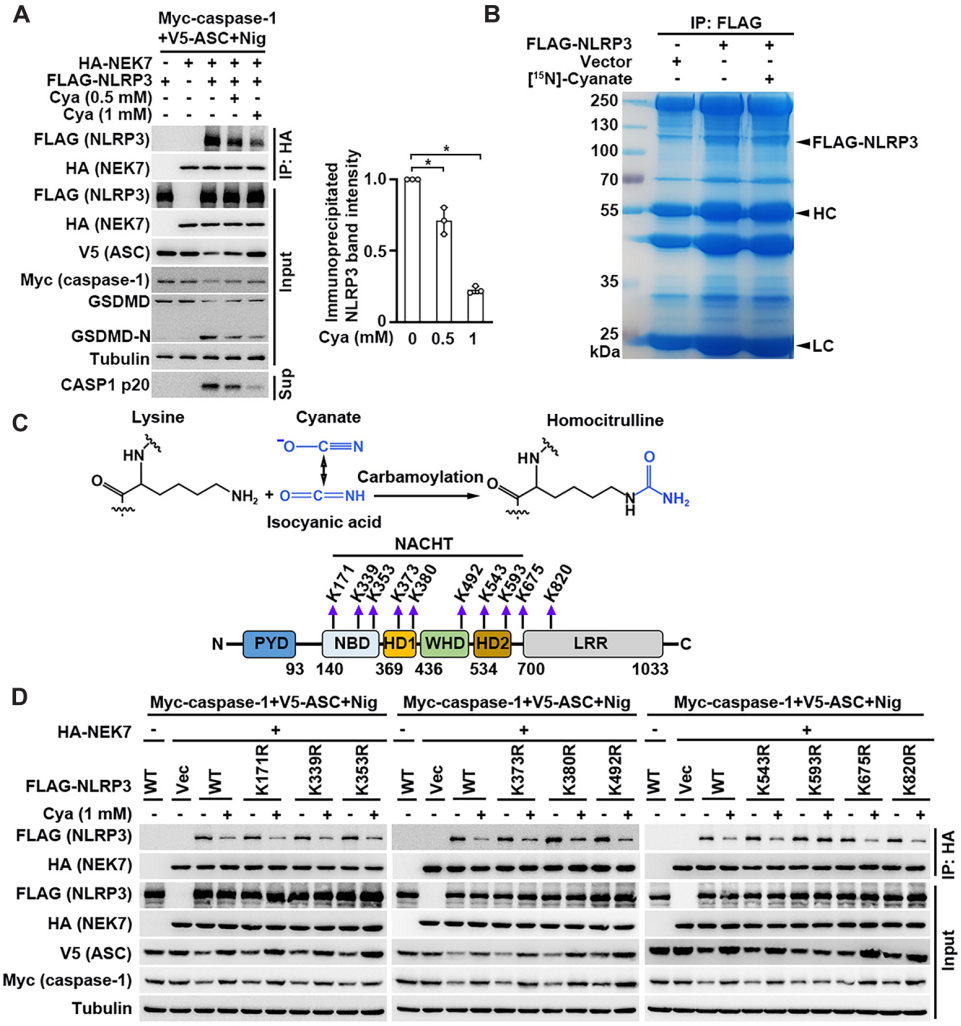

Fig. 3. Carbamoylation sites on NLRP3 are identified, and their effects on NLRP3-NEK7 interaction are evaluated. (**A**) 293T cells stably expressing GSDMD were cotransfected with plasmids expressing indicated proteins. Twenty-four hours after transfection, the cells were incubated with indicated concentrations of cyanate for 30 min and then treated with Nig for another 45 min. Immunoprecipitation was performed using an anti-HA antibody followed by an immunoblotting analysis (left panel). Cyanate-mediated disruption of NLRP3-NEK7 interaction was quantified and presented as mean ± SD of three independent experiments (right panel). *P* values were calculated using one-way ANOVA. **P* < 0.01. (**B**) FLAG-NLRP3 immunoprecipitated from the lysate of FLAG-NLRP3–overexpressing iBMDMs treated with ^{15}N-labeled cyanate (1 mM) for 1 hour was separated through SDS-PAGE and stained with Coomassie brilliant blue. The indicated protein band matching the molecular weight of FLAG-NLRP3 was excised for MS analysis. HC, heavy chain; LC, light chain. (**C**) Schematic illustration of carbamoylation reaction (top) and carbamoylated lysine (K) residues on NLRP3 (bottom) was indicated. (**D**) 293T cells were cotransfected with plasmids expressing FLAG-tagged WT or indicated NLRP3 mutants, HA-NEK7, V5-ASC, and Myc-caspase-1. Twenty-four hours after transfection, the cells were incubated with cyanate (1 mM) for 30 min and then treated with Nig for another 45 min. Immunoprecipitation was performed using an anti-HA antibody followed by an immunoblotting analysis.

resistant (r) NLRP3 (rNLRP3) or rNLRP3 K593R mutant (Fig. 4E). As expected, LPS-induced NLRP3 K593ca was observed in WT human (h) or mouse (m) rNLRP3 (h/mrNLRP3)–expressed, but not h/mrNLRP3 K593R–expressed, THP-1 cells and iBMDMs, as detected by immunoblotting analysis (Fig. 4F). Moreover, an increase of LPS-Nig/ATP–induced interaction between NLRP3 and NEK7 was observed in h/mrNLRP3 K593R–expressed THP-1 cells and iBMDMs compared to the cells expressing WT h/mrNLRP3 (Fig. 4G). Together, these data suggest that isocyanic acid carbamoylates NLRP3 at K593 to disrupt the interaction between NLRP3 and NEK7 upon NLRP3 inflammasome activation.

NLRP3 K593ca is required to limit NLRP3 inflammasome activation

We next investigated the role of NLRP3 K593ca in NLRP3 inflammasome activation. As expected, reconstituted expression of h/mrNLRP3 K593R mutant promoted LPS-Nig/ATP–induced releases of IL-1β (Fig. 5A), IL-18 (Fig. 5B), and LDH (Fig. 5C); cleavages of IL-1β and caspase-1 to their active forms (Fig. 5D); and GSDMD-N formation (Fig. 5E). Furthermore, reconstituted expression of h/mrNLRP3 K593R mutant also promoted LPS-Nig/ATP–induced formation of large multimeric ASC complexes (Fig. 5F). However, the exacerbated NLRP3 inflammasome activation resulting from

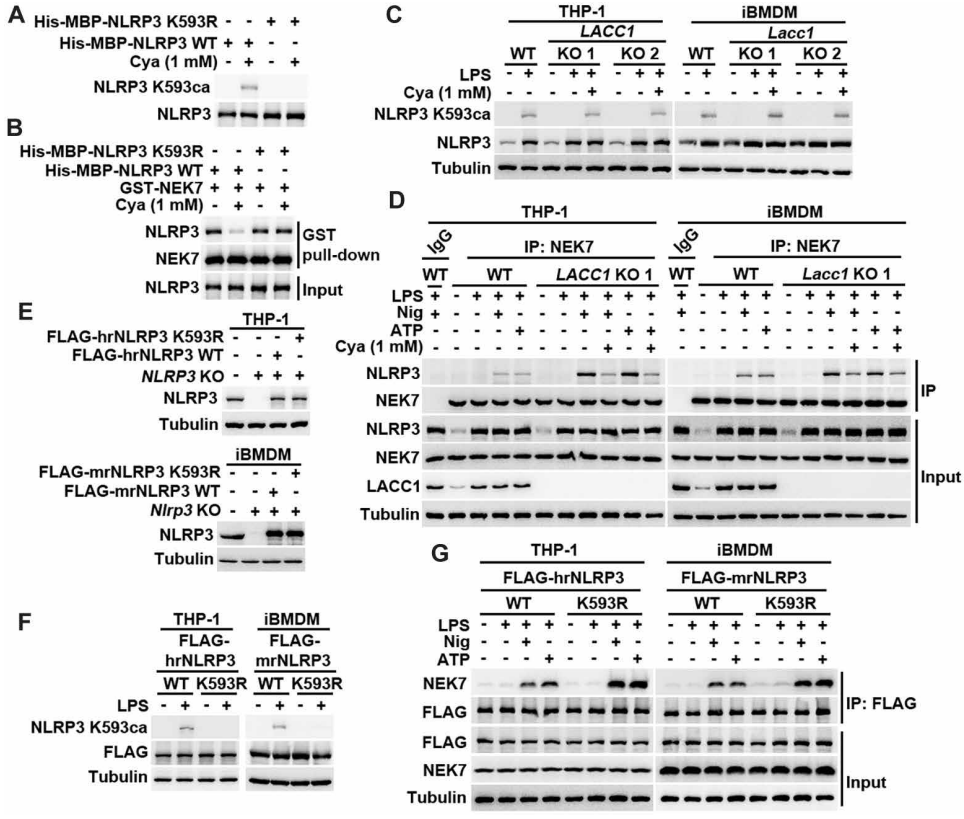

Fig. 4. Isocyanic acid carbamoylates NLRP3 at K593 to disrupt the interaction between NLRP3 and NEK7. (**A**) Purified His-MBP–tagged WT NLRP3 or NLRP3 K593R was incubated with cyanate (1 mM) for 1 hour. NLRP3 K593ca was detected by immunoblotting. (**B**) In vitro carbamoylation assay was performed by incubating cyanate (1 mM) with purified WT His-MBP-NLRP3 or His-MBP-NLRP3 K593R for 1 hour. Samples were then mixed with GST-NEK7. A GST pull-down assay was performed followed by immunoblotting with the indicated antibodies. (**C** and **D**) WT and *LACC1*/*Lacc1*-KO THP-1 cells and iBMDMs were stimulated with LPS (100 ng ml^{-1}) for 8 hours. The LPS-primed macrophages were incubated without or with 1 mM cyanate for 30 min, and NLRP3 K593ca was detected by immunoblotting (C). The LPS-primed macrophages were pretreated without or with 1 mM cyanate for 30 min and incubated with 10 μM Nig or 5 mM ATP for another 45 min, and then immunoprecipitation was performed using an anti-NEK7 antibody (D). (**E**) FLAG-tagged WT h/mrNLRP3 or h/mrNLRP3 K593R was reconstitutively expressed in THP-1 cells and iBMDMs with the KO of endogenous *NLRP3*/*Nlrp3*. Immunoblotting was performed using indicated antibodies. hrNLRP3, human rNLRP3; mrNLRP3, mouse rNLRP3. (**F** and **G**) *NLRP3*/*Nlrp3*-KO THP-1 cells and iBMDMs with reconstituted expression of FLAG-tagged WT h/mrNLRP3 or h/mrNLRP3 K593R were stimulated with LPS (100 ng ml^{-1}) for 8 hours. NLRP3 K593ca was detected by immunoblotting (F). The LPS-primed macrophages were incubated with 10 μM Nig or 5 mM ATP for another 45 min, and then immunoprecipitation was performed using an anti-FLAG antibody (G).

reconstituted expression of K593ca-deficient h/mrNLRP3 mutant was not influenced by treatment with 1 mM cyanate (Fig. 5, A to F). Of note, WT h/mrNLRP3– and h/mrNLRP3 K593R–expressed THP-1 cells and iBMDMs have similar levels of LACC1 expression (fig. S6H) and isocyanic acid production (fig. S6I) upon LPS stimulation. These data suggest that isocyanic acid–mediated NLRP3 K593ca is required to limit NLRP3 inflammasome activation.

To further characterize the effect of NLRP3 K593ca on NLRP3 inflammasome activation, LPS-primed THP-1 cells and iBMDMs with KO of endogenous *NLRP3*/*Nlrp3* and reconstituted expression of WT h/mrNLRP3 or K593ca-deficient h/mrNLRP3 K593R mutant were treated with increasing concentrations of Nig, ATP, and MSU crystals for a certain time duration (Nig and ATP for 45 min; MSU crystals for 60 min). NLRP3 K593ca deficiency induced a similar fold change of IL-1β release in LPS-primed THP-1 cells and iBMDMs upon treatments with different concentrations of Nig, ATP, and MSU crystals (fig. S6J). Likewise, NLRP3 K593ca deficiency induced a similar fold change of IL-1β release in LPS-primed THP-1 cells and iBMDMs upon treatments with Nig (10 μM), ATP (5 mM), and MSU crystals (300 μg ml^{-1}) for different time durations (fig. S6K). These data support that NLRP3 K593ca is required to limit inflammasome activation triggered by different NLRP3 activators within a wide range of doses and durations of treatment time.

In addition, to ascertain whether LACC1 regulates NLRP3 inflammasome activation in a priming time–dependent manner, we primed WT and *LACC1*/*Lacc1*-KO THP-1 cells and iBMDMs with different stimuli, including Toll-like receptor 4 (TLR4) agonist LPS and TLR1/2 agonist pam3CSK4 (*33*) for different time durations. In line with the results shown in fig. S1A, full induction of LACC1 expression and NLRP3 K593ca was observed upon stimulation with LPS or pam3CSK4 for 8 hours in WT, but not *LACC1*/*Lacc1*-KO, THP-1 cells and iBMDMs (fig. S7A). Furthermore, *LACC1*/*Lacc1* KO increased the releases of IL-1β when these cells were stimulated with LPS or pam3CSK4 for 6, 8, and 10 hours, but not 3 hours, before activation of NLRP3 inflammasome with Nig (fig. S7B). Of note, similar results were observed when the WT and *LACC1*/*Lacc1*-KO THP-1 cells and iBMDMs were stimulated with a double concentration of LPS or pam3CSK4 (fig. S7, C and D). Together, these

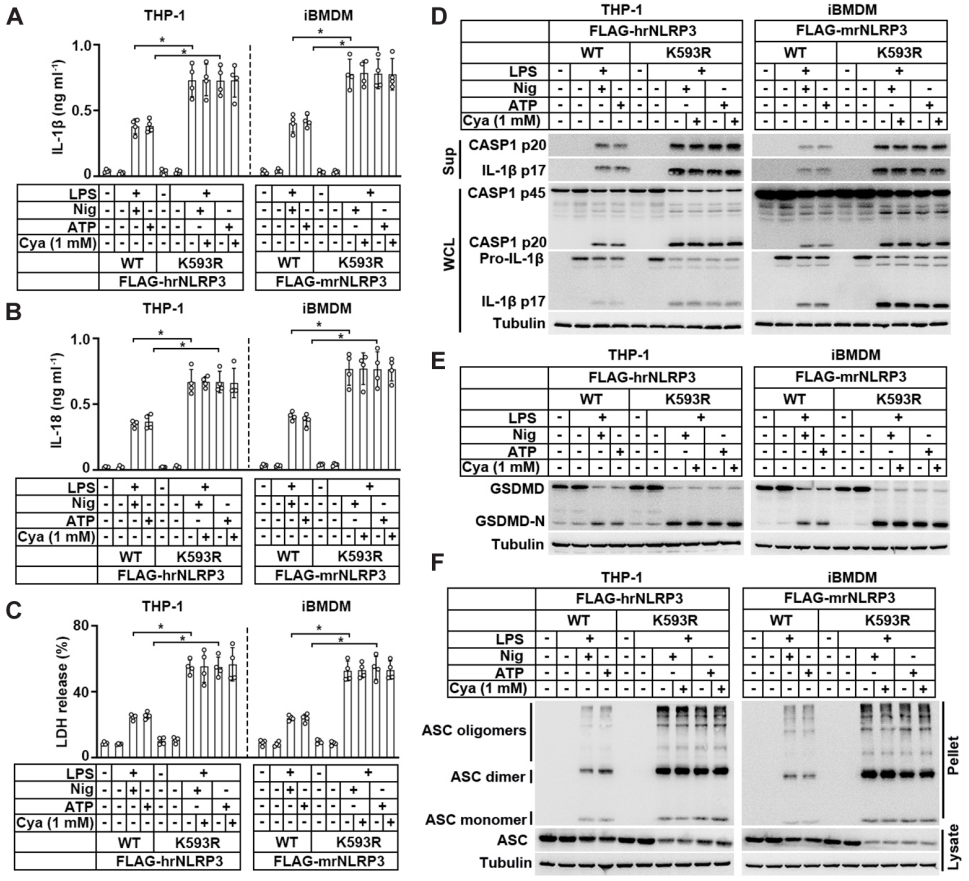

Fig. 5. NLRP3 K593ca limits NLRP3 inflammasome activation. (**A** to **F**) *NLRP3*/*Nlrp3*-KO THP-1 cells and iBMDMs with reconstituted expression of FLAG-tagged WT h/mrNLRP3 or h/mrNLRP3 K593R were stimulated with LPS (100 ng ml^{-1}) for 8 hours. The LPS-primed macrophages were pretreated without or with 1 mM cyanate for 30 min and then incubated with 10 μM Nig or 5 mM ATP for another 45 min. *P* values were calculated using a two-tailed Student's *t* test (A to C). $*P < 0.01$. (A to C) The release of IL-1β (A), IL-18 (B), and LDH (C) in culture supernatants was determined by ELISA. The data are presented as mean ± SD of four independent experiments. (D) Pro- and mature caspase-1 and IL-1β protein in the cell lysates were analyzed by immunoblotting. (E) Cleavage of GSDMD was analyzed by immunoblotting. (F) The formation of large multimeric ASC complexes was analyzed by immunoblotting.

data suggest that LACC1 limits NLRP3 inflammasome activation in a priming time–dependent manner.

Isocyanic acid–mediated NLRP3 K593ca limits inflammatory response in vivo

To further investigate the role of isocyanic acid–mediated NLRP3 K593ca in inflammatory response in vivo, we used a mouse model of sepsis in which LPS was intraperitoneally injected into mice to analyze the inflammatory response of mouse to LPS injection. *Lacc1*$^{-/-}$ mice (fig. S8A) and *Nlrp3* K593R-knockin (KI) mice, which are referred to as *Nlrp3* K593R mice (fig. S8B), were validated by genotyping. In line with the results from in vitro NLRP3 inflammasome activation assays, *Lacc1*$^{-/-}$ mice and *Nlrp3* K593R mice exhibited poor survival rates (Fig. 6A), elevated serum levels of IL-1β (Fig. 6B) and IL-18 (Fig. 6C), and increased clinical score (Fig. 6D), compared with their WT siblings after LPS injection. However, the poor survival rate (Fig. 6A) and exacerbated inflammatory response (Fig. 6, B to D) observed in *Lacc1*$^{-/-}$ mice were abrogated by co-injection of LPS with cyanate (100 mg kg^{-1}). Furthermore, LACC1 expression (fig. S8C), NLRP3 K593ca (fig. S8C), and intracellular isocyanic acid (fig. S8D) were detected in *Lacc1*$^{+/+}$, but not *Lacc1*$^{-/-}$, peritoneal macrophages isolated from mice injected with LPS. By contrast, when *Lacc1*$^{-/-}$ mice were co-injected with LPS and cyanate, *Lacc1*$^{-/-}$ peritoneal macrophages isolated from these mice displayed a level of NLRP3 K593ca (fig. S8C) and intracellular isocyanic acid (fig. S8D) akin to that in *Lacc1*$^{+/+}$ peritoneal macrophages isolated from mice injected with LPS. Likewise, NLRP3 K593ca was detected in WT, but not *Nlrp3* K593R, peritoneal macrophages isolated from mice injected with LPS (fig. S8E), although similar levels of LACC1 expression (fig. S8E) and intracellular isocyanic acid (fig. S8F) were detected in these cells. These data suggest that isocyanic acid–mediated NLRP3 K593ca is required to limit inflammatory response to LPS in vivo.

Next, we used another mouse model of gout in which MSU crystals, the agent activating NLRP3 inflammasome, were intraperitoneally injected into mice to analyze the inflammatory response of mouse to injection of MSU crystals. Consistent to the results from the mouse model of sepsis, *Lacc1*$^{-/-}$ mice and *Nlrp3* K593R mice exhibited elevated serum levels of IL-1β (Fig. 6E) and IL-18 (Fig. 6F), and increased neutrophil number in the peritoneal lavage fluid (Fig. 6G), compared with their *Lacc1*$^{+/+}$ or WT siblings after injection of MSU crystals (30 mg kg^{-1}). Co-injection of MSU crystals with cyanate (100 mg kg^{-1}) abrogated the exacerbated inflammatory

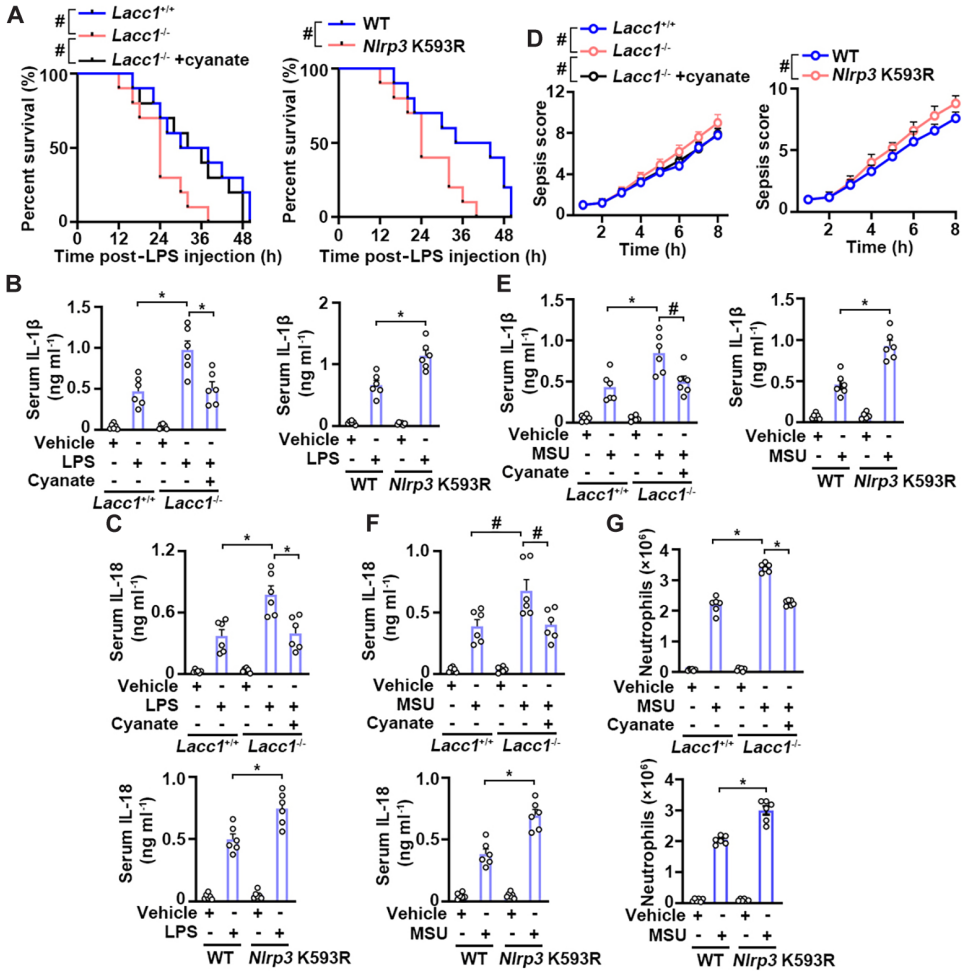

Fig. 6. Isocyanic acid–mediated NLRP3 K593ca limits inflammatory response in vivo. (**A** to **D**) LPS (10 mg kg^{-1} in 200 μl of PBS), (**E** to **G**) MSU crystals (30 mg kg^{-1} in 200 μl of PBS), or vehicle (200 μl of PBS) (A to G) were intraperitoneally injected into *Lacc1*$^{+/+}$ and *Lacc1*$^{-/-}$ mice, WT, and *Nlrp3* K593R mice. (A to G) *Lacc1*$^{-/-}$ mice were co-injected with LPS or MSU with cyanate [LPS (10 mg kg^{-1}) or MSU crystals (30 mg kg^{-1}) combined with cyanate (100 mg kg^{-1}) in 200 μl of PBS]. *P* values were calculated using the two-tailed log-rank test (A), two-tailed Student's *t* test (B, C, and E to G), or linear mixed model (D). Means ± SEM are shown (B to G). $^{*}P < 0.01$, $^{\#}P < 0.05$. (A) Survival of mice ($n = 10$) was monitored after LPS injection. (B and C) Serum IL-1β (B) and IL-18 (C) levels of mice ($n = 6$) were measured 8 hours after LPS injection. (D) Clinical scores for sepsis severity (maximum score, 15) of mice ($n = 10$) were shown 8 hours after LPS injection. (E to G) Serum IL-1β (E) and IL-18 (F) levels of mice ($n = 6$) and neutrophil number (G) in the peritoneal lavage fluid of mice ($n = 6$) were measured 8 hours after MSU crystal injection.

response observed in *Lacc1*$^{-/-}$ mice (Fig. 6, E to G). As expected, LACC1 expression (fig. S8G), NLRP3 K593ca (fig. S8G), and intracellular isocyanic acid (fig. S8H) were detected in *Lacc1*$^{+/+}$, but not *Lacc1*$^{-/-}$, peritoneal macrophages isolated from mice injected with MSU crystals. However, when *Lacc1*$^{-/-}$ mice were co-injected with MSU crystals and cyanate, *Lacc1*$^{-/-}$ peritoneal macrophages isolated from these mice displayed a level of NLRP3 K593ca (fig. S8G) and intracellular isocyanic acid (fig. S8H) akin to that in *Lacc1*$^{+/+}$ peritoneal macrophages isolated from mice injected with MSU crystals. Likewise, NLRP3 K593ca was detected in WT, but not *Nlrp3* K593R, peritoneal macrophages isolated from mice injected with MSU crystals (fig. S8I), although similar levels of LACC1 expression (fig. S8I) and intracellular isocyanic acid (fig. S8J) were detected in these cells. These data suggest that isocyanic acid–mediated NLRP3 K593ca is required to limit inflammatory response to MSU crystals in vivo.

Finally, to validate the suppressive effect of NLRP3 K593ca on NLRP3 inflammasome activation in primary macrophages, we isolated WT and *Nlrp3* K593R mBMDMs from WT and *Nlrp3* K593R mice, respectively. The purity of these mBMDMs was at least 98%, as revealed by flow cytometry analysis (Fig. 7A). As expected, LPS-induced NLRP3 K593ca was observed in WT, but not *Nlrp3* K593R, mBMDMs (Fig. 7B). In addition, an increase of LPS-Nig/ATP–induced interaction between NLRP3 and NEK7 was also observed in *Nlrp3* K593R mBMDMs compared to the WT mBMDMs (Fig. 7C). Accordingly, *Nlrp3* K593R mBMDMs manifested exacerbated NLRP3 inflammasome activation, as evidenced by the observations that *Nlrp3* K593R KI promoted LPS-Nig/ATP–induced releases of IL-1β (Fig. 7D), IL-18 (Fig. 7E), and LDH (Fig. 7F); cleavages of IL-1β and caspase-1 to their active forms (Fig. 7G); formation of GSDMD-N (Fig. 7H); and large multimeric ASC complexes (Fig. 7I) in mBMDMs. Nevertheless, WT and *Nlrp3* K593R mBMDMs displayed similar levels of LACC1 expression (Fig. 7J) and intracellular isocyanic acid (Fig. 7K) upon LPS stimulation. These results demonstrate that NLRP3 K593ca may limit NLRP3 inflammasome activation in inflammatory primary macrophages.

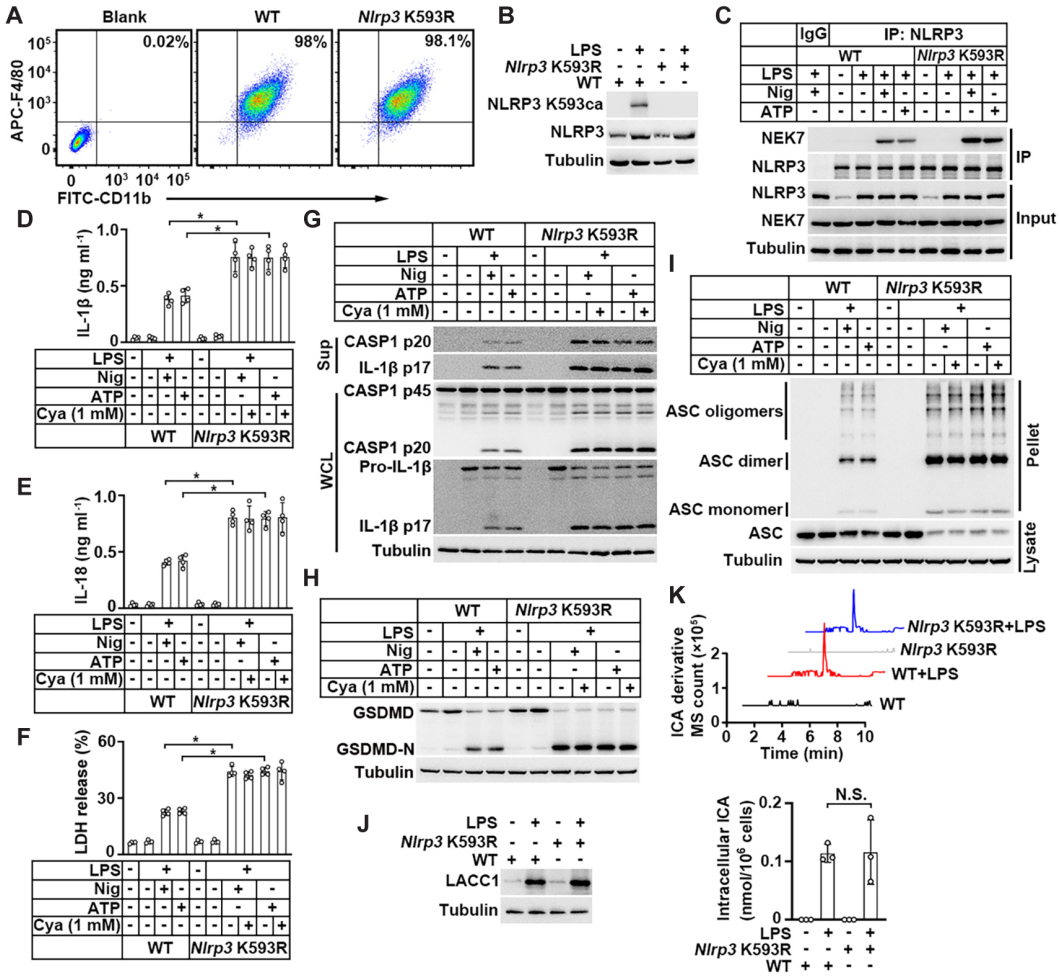

Fig. 7. Deficiency of NLRP3 K593ca exacerbates NLRP3 inflammasome activation in primary macrophages. (**A** to **K**) Isolated WT and *Nlrp3* K593R mBMDMs (A) were stimulated with LPS (100 ng ml^{-1}) for 8 hours (B to K). The LPS-primed macrophages were pretreated without or with 1 mM cyanate for 30 min and then incubated with 10 μM Nig or 5 mM ATP for another 45 min (C to I). *P* values were calculated using a two-tailed Student's *t* test (D to F and K). N.S., not significant. *$P < 0.01$. (A) Flow cytometry analysis of mBMDMs isolated from WT or *Nlrp3* K593R mouse littermates using antibodies against macrophage surface markers CD11b and F4/80. Purity of the isolated macrophages obtained from representative mouse was shown. Isolated WT mBMDMs without staining with antibodies served as a blank control. (B) NLRP3 K593ca was detected by immunoblotting. (C) Immunoprecipitation was performed using an anti-NLRP3 antibody. The immunoprecipitated protein complexes were analyzed by immunoblotting. (D to F) The release of IL-1β (D), IL-18 (E), and LDH (F) in culture supernatants was determined by ELISA. The data are presented as mean ± SD of four independent experiments. (G) Pro- and mature caspase-1 and IL-1β protein in the lysates of mBMDMs were analyzed by immunoblotting. (H) Cleavage of GSDMD was analyzed by immunoblotting. (I) The formation of large multimeric ASC complexes was analyzed by immunoblotting. (J) LACC1 levels were detected by immunoblotting. (K) Intracellular isocyanic acid levels were detected by LC-MS analysis. The data are presented as mean ± SD of three independent experiments.

DISCUSSION

It is well known that NLRP3 inflammasome signaling is associated to a wide range of different autoinflammatory diseases, for example, Alzheimer's disease and rheumatoid arthritis (*34*), highlighting the importance of further understanding the precise mechanism by which NLRP3 inflammasome is activated and regulated. Here, we show that isocyanic acid, an endogenous metabolite generated by LACC1-catalyzed cleavage of citrulline, carbamoylates NLRP3 at K593 to disrupt the interaction between NLRP3 and NEK7, two key components of NLRP3 inflammasome complex, and subsequently limits the NLRP3 inflammasome activation in the LPS-primed macrophages. Therefore, our study demonstrates that isocyanic acid is a repressor of NLRP3 inflammasome.

NLRP3 and NEK7 form a complex upon NLRP3 inflammasome activation, and the interactions between NLRP3 and NEK7 occur at multiple surfaces in the LRR and NACHT domains of NLRP3 (*4*). It has been reported that 4-octyl itaconate, a derivative of itaconate, blocked the interaction between NLRP3 and NEK7 by dicarboxypropylating NLRP3 at C548 (*35*), an amino acid residue located in the helical domain 2 (HD2) of NLRP3 and one of the surfaces at which NLRP3 interacts with NEK7 (*4*). In line with these studies, our data show that isocyanic acid disrupts the interaction between NLRP3 and NEK7 by carbamoylating NLRP3 at K593, a site that is also located in the HD2 of NLRP3, demonstrating that posttranslational modifications of NLRP3 HD2 may be important in regulating inflammasome function.

It has been reported that LACC1 is a metabolic enzyme catalyzing isocyanic acid production from citrulline (*17*) and LACC1 expression is up-regulated in inflammatory macrophages (*11*, *12*). Our study revealed that intracellular levels of isocyanic acid were dramatically up-regulated in THP-1 cells and iBMDMs upon LPS stimulation for 8 hours (Fig. 2A). In addition, intracellular isocyanic acid was undetectable when cyanase was expressed in these cells (fig. S2, F and G), suggesting that our method for detecting intracellular isocyanic acid is reliable. Furthermore, it is noteworthy that exogenous cyanate, as a small-molecule metabolite, must traverse the cellular plasma membrane to exert its regulatory effect on intracellular proteins. Our study demonstrates that high concentration (1 mM) of exogenous cyanate is needed to replenish intracellular isocyanic acid to the levels comparable to that synthesized by LACC1 in inflammatory macrophages, implying the low import efficiency for exogenous cyanate in these cells.

Previous studies reported that cyanate and its tautomer isocyanic acid can be generated via the spontaneous decomposition of urea in aqueous solutions (*20*, *36*) or MPO-catalyzed oxidation of thiocyanate (*37*). Our results demonstrated that intracellular urea elimination by urease expression did not exert obvious impact on LACC1-dependent isocyanic acid production (fig. S5, A to C) and MPO expression was undetectable in inflammatory macrophages (fig. S5D). Moreover, the LPS-induced increase of intracellular isocyanic acid levels was abolished by *LACC1*/*Lacc1* KO (Fig. 2A). These data strongly support that LPS induces isocyanic acid production in a LACC1-dependent manner in inflammatory macrophages.

Additionally, it was reported that *LACC1* KO did not significantly alter the levels of IL-1β secreted from U937 cells and macrophages obtained from healthy donors and JIA patients harboring loss-of-function *LACC1* mutations displayed similar levels of IL-1β secretion when these cells were stimulated with LPS for 3 hours before activation of NLRP3 inflammasome with Nig (*14*). In line with these results, we found that there was no induction of LACC1 expression in THP-1 cells and iBMDMs stimulated with LPS for 3 hours (figs. S1A and S7, A and C). Accordingly, these findings imply that LACC1 may not affect NLRP3 inflammasome activation in macrophages primed with LPS for 3 hours.

In conclusion, our study unveils an immunoregulatory function of isocyanic acid, that is, to attenuate inflammation by limiting the NLRP3 inflammasome activation in macrophages. Elucidating the anti-inflammatory roles of isocyanic acid would provide us with a comprehensive understanding of the regulatory mechanisms underlying NLRP3 inflammasome activation, which warrants further in-depth investigations.

MATERIALS AND METHODS

Materials

Rabbit polyclonal antibodies against NLRP3 K593ca were obtained from Affinity Biosciences (Jiangsu, China). The polyclonal antibodies recognizing NLRP3 K593ca were generated by immunizing a rabbit with an NLRP3 K593ca peptide (ERTSYLEK[Kca]LSCKIS) conjugated to keyhole limpet hemocyanin (KLH) via the cysteine (C) residue. The rabbit serum was collected and purified with an affinity column conjugated with NLRP3 K593 peptide (ERTSYLEKKLSCKIS) without carbamoylation followed by binding to an affinity column conjugated with the NLRP3 K593ca peptide (ERTSYLEK[Kca] LSCKIS). The bound antibodies were then eluted and concentrated. A working concentration of 1 μg ml^{-1} was used for immunoblotting analyses.

Primary antibodies recognizing NLRP3 (#15101), hemagglutinin (HA) tag (#3724), ASC/TMS1 (#67824), V5 tag (#13202), Myc tag (#2278), GSDMD (#97558), IKKβ (#2678), and caspase-1 (#2225) were purchased from Cell Signaling Technology. Goat polyclonal antibodies recognizing mouse IL-1β (#AF-401) and MPO (#AF3667) were purchased from R&D Systems. Mouse monoclonal antibodies recognizing mouse caspase-1 (#AG-20B-0042-C100) were purchased from Adipogen. Rabbit monoclonal antibodies recognizing NEK7 (#ab133514), GSDMD (#ab209845), human IL-1β (#ab254360), ASC/TMS1 (#ab155970), ERGIC-53 (#ab125006), and GFP (#ab290) were obtained from Abcam. Mouse monoclonal antibodies recognizing tubulin (#sc-23948) and LACC1 (#sc-376231) were obtained from Santa Cruz Biotechnology. Antibody against GM130 (#610822) was purchased from BD Biosciences. Antibody recognizing TGN38 (#66477-1-Ig) was obtained from Proteintech. Mouse monoclonal antibodies against FLAG tag (#F3165), anti-FLAG M2 affinity gel (#A2220), phenylmethylsulfonyl fluoride (PMSF) (#P7626), leupeptin (#L2884), IPTG (isopropyl-β-D-thiogalactopyranoside) (#I6758), potassium cyanate (#215074), potassium cyanate-^{15}N (#609358), LPS (#L7895), ornithine (#57197), citrulline (#C7629), arginine (#A8094), and 2,4(1*H*,3*H*)-quinazolinedione (#142026) were purchased from Sigma-Aldrich. Citrulline (ureido-^{13}C) (#CLM-4899-PK) was purchased from Cambridge Isotope Laboratories. Nig (#tlrl-nig), poly(dA:dT) (#tlrl-patn), flagellin (#tlrl-pafla), MSU crystals (#tlrl-msu), and pam3CSK4 (#tlrl-pms) were purchased from InvivoGen. Allophycocyanin (APC) anti-mouse F4/80 (#123115), fluorescein isothiocyanate (FITC) anti-mouse/human CD11b (#101205), APC/Cyanine7 anti-mouse Ly6G (#127623), and Pacific Blue anti-mouse CD45.2 (#109819) were purchased from BioLegend. Goat anti-rabbit immunoglobulin G (IgG) (H+L) cross-adsorbed secondary antibody (Alexa Fluor 488) (#A-11008), 30-kDa spin column (#88529), EDTA-free protease inhibitors cocktail (#A32965), glutathione agarose (#16100), 4′,6-diamidino-2-phenylindole (DAPI) (#D8417), TRIzol (#15596018), Opti-MEM (#31985062), and Lipofectamine 2000 (#11668019) were obtained from Thermo Fisher Scientific. Bis(sulfosuccinimidyl)suberate (BS^3) (#M9872) was obtained from Abmole. 2-Aminobenzoic acid sodium salt (#A921866) was purchased from Macklin. EasyBlot anti-rabbit (#GTX221666- 01) and anti-mouse IgG [horseradish peroxidase (HRP)] (#GTX221667-01) were purchased from GeneTex. HRP-labeled goat anti-rabbit IgG (H+L) (#A0208) was obtained from Beyotime. ClonExpress MultiS One Step cloning kit (#C113-02) and 2 × Phanta Max Master mix (#P515) were obtained from Vazyme Biotech. Spe I restriction enzyme (#R3133) was purchased from New England Biolabs. Unmodified peptides (ERTSYLEKKLSCKIS and ERTSYLEKRLSCKIS) were obtained from ChinaPeptides, and carbamoylated peptide (ERTSYLEK[Kca]LSCKIS) was obtained from Wu Xi App Tec.

Methods

Cell lines and cell culture conditions

THP-1 cells were obtained from American Type Culture Collection (ATCC) and cultured in RPMI 1640 supplemented with 10% heat-inactivated and dialyzed fetal bovine serum (FBS) (Gibco) and penicillin-streptomycin (100 μg ml^{-1}). iBMDMs, 293T cells, and 293FT cells were cultured in Dulbecco's modified Eagle's medium (DMEM) supplemented with 10% heat-inactivated and dialyzed FBS (Gibco) and penicillin-streptomycin (100 μg ml^{-1}). The cells were

cultured in 5% CO_2 at 37°C and routinely tested for mycoplasma contamination and authenticated by short tandem repeat (STR) profiling. The monocytic THP-1 cells were differentiated into macrophages by incubation with phorbol 12-myristate 13-acetate (PMA) (100 ng ml^{-1}) for 2 days before the downstream experiments. Unless stated, the LPS (Sigma #L7895) concentration used for treatments was 100 ng ml^{-1}.

Generation of Lacc1-KO and Nlrp3 K593R-KI mice

Lacc1$^{+/-}$ mice (strain #T033882) on a C57BL/6J background were purchased from GemPharmatech. The heterozygous *Lacc1*$^{+/-}$ mice were intercrossed to generate homozygous *Lacc1*$^{-/-}$ mice. Heterozygous *Nlrp3* K593R-KI mice (referred as *Nlrp3* K593R mice) on a C57BL/6J background were generated via CRISPR-Cas9–mediated genomic editing (GemPharmatech). In brief, gRNA (target sequence: 5′-CCAGGAGAGAACCTCTTATT-3′) was designed to target the genomic area adjacent to *Nlrp3* K593R mutation site. The purified active Cas9, gRNA, and a single-stranded donor oligonucleotide, which was used as a template to introduce the codon mutation of AAA to AGG to create *Nlrp3* K593R mutation and two synonymous codon mutations of ACC to ACT and TCT to AGT to prevent the recutting by Cas9, were co-injected into zygotes for production of *Nlrp3* K593R mice. The heterozygous *Nlrp3* K593R mice were intercrossed to generate homozygous *Nlrp3* K593R mice. Mouse siblings at the ages between 6 and 8 weeks were used for NLRP3-associated inflammatory response experiments.

All mice were housed under 23 ± 2°C temperature and 50 to 65% humidity in specific pathogen–free environment with a 12-hour light/dark cycle. The mice were euthanized by CO_2 from compressed gas cylinders. All animal experimental protocols were approved by the Institutional Animal Care and Use Committee of the Institute of Biophysics, Chinese Academy of Sciences, under approval number SYXK2019030.

Mouse genotyping

To extract mouse DNA genotyping, a small piece of mouse toe (~10 mg) was clipped and heated at 98°C for 30 min in 100 μl of 50 mM NaOH solution. The samples were mixed with equal volume (100 μl) of double-distilled water and 10 μl of neutralizing reagent (1 M tris-HCl, pH 8.0) and centrifuged at 13,200*g* for 10 min, and then the supernatants were collected and used as templates for the downstream PCR amplifications. For *Nlrp3* K593R mice, a pair of primer spanning the *Nlrp3* K593R mutation area was used for PCR amplifications. The PCR amplicons were digested with restriction enzyme Spe I for 1 hour at 37°C followed by agarose gel electrophorese. In addition, the sequences of PCR amplicons were determined by Sanger sequencing. For *Lacc1*$^{-/-}$ mice, the genotyping was performed according to the instructions provided by GemPharmatech. For PCR amplicon 1, a PCR product with a size of 374 base pairs (bp) was obtained when the samples of DNA extracted from *Lacc1*$^{+/+}$ or *Lacc1*$^{+/-}$, but not *Lacc1*$^{-/-}$, mice were used as templates. For PCR amplicon 2, a PCR product with a size of 965 bp was obtained when the samples of DNA extracted from *Lacc1*$^{-/-}$ or *Lacc1*$^{+/-}$, but not *Lacc1*$^{+/+}$, mice were used as templates. The sequences of PCR primers used for mouse genotyping were listed in table S1.

Murine bone marrow extraction and differentiation of mBMDMs

Bone marrow cells (BMCs) were isolated from 6-week-old male *Nlrp3* K593R mice and their WT littermates. BMCs were flushed from tibia and femur bones with cold DMEM under an aseptic condition. The BMCs were collected and filtered using a 70-μm cell strainer. The cells were harvested by centrifugation at 600*g* for 5 min and then incubated in ACK lysing buffer (150 mM NH_4Cl, 10 mM $KHCO_3$, 0.1 mM EDTA, pH 7.4) for 3 min at room temperature to remove red blood cells. After washing twice with ice-cold phosphate-buffered saline (PBS), the BMCs were seeded into six-well plates (5×10^5 per well) containing 2 ml of differentiation medium [DMEM supplemented with 10% ultralow endotoxin FBS, 2 mM L-glutamine, penicillin (100 μg ml^{-1}), streptomycin (100 μg ml^{-1}), and macrophage colony-stimulating factor (20 ng ml^{-1}) (PeproTech #AF-315-02)]. The cells were differentiated for 7 days with replacement of fresh differentiation medium every 3 days. The resultant mBMDMs were harvested and used for downstream experiments.

LPS-induced sepsis model

Nlrp3 K593R mice, *Lacc1*$^{-/-}$ mice, and their WT/*Lacc1*$^{+/+}$ siblings at the ages between 6 and 8 weeks were intraperitoneally injected with LPS (Sigma #L7895) (10 mg kg^{-1} in 200 μl of PBS) without or with cyanate (100 mg kg^{-1}). For cytokine measurements, the blood samples were collected 8 hours after LPS injection and serum levels of IL-1β and IL-18 were measured by ELISA kits according to the manufacturer's instructions. For survival studies, the survival status of each mouse was monitored and recorded every 2 hours. Clinical severity of the LPS-injected mice was evaluated by a graded scoring system with minor modifications (*38*). Clinical sepsis severity, quantified with breathing pattern score (0 to 5), activity and movement score (0 to 5), and appearance score (0 to 5), was recorded every 60 min for up to 8 hours after LPS injection.

Peritonitis model induced by MSU crystals

Nlrp3 K593R mice, *Lacc1*$^{-/-}$ mice, and their WT/*Lacc1*$^{+/+}$ siblings at the ages between 6 and 8 weeks were intraperitoneally injected with MSU crystals (30 mg kg^{-1} in 200 μl of PBS) without or with cyanate (100 mg kg^{-1}). Eight hours after injection of MSU crystals, the mice were euthanized in a CO_2 chamber. Peritoneal cells were collected by flushing the peritoneal cavities of mice with 4 ml of ice-cold PBS under an aseptic condition. The suspension of peritoneal cells was centrifuged at 500*g* for 5 min at 4°C. The cell pellets were collected, resuspended in 0.5 ml of cold PBS, and passed through a 70-μm filter. Peritoneal cells were stained with fluorescent dye–conjugated antibodies against neutrophil surface markers (CD45, CD11b, and Ly6G) and then loaded onto a BD LSRFortessa flow cytometer equipped with FlowJo software. The remaining peritoneal cells were counted using a TC20 automated cell counter (Bio-Rad). The number of neutrophils in peritoneal lavage fluid was calculated by multiplying the total peritoneal cell count with the percentage of neutrophils in each sample.

Plasmid construction and mutagenesis

gRNAs targeting *LACC1*/*Lacc1* or *NLRP3*/*Nlrp3* were designed using an online tool (https://www.zlab.bio/resources). Two predicted gRNAs with high KO efficiency were chosen and cloned into the lentiCRISPRv2 vector (Addgene #98290) with a selection marker of puromycin. The open reading frames (ORFs) of *Nek7* [National Center for Biotechnology Information (NCBI) sequence NM_021605.5], *Asc* (NCBI sequence NM_023258.4), *Caspase 1* (NCBI sequence NM_009807.2), *Nlrp3* (NCBI sequence NM_145827.4), and *Gsdmd* (NCBI sequence NM_026960.4) were amplified by PCR from a cDNA library derived from iBMDMs and subcloned into plasmid vectors including pcDNA3.1, pGEX-4 T1, or lenti-CMV (cytomegalovirus) (lentiviral vector with hygromycin resistance). The coding sequence of NLRP3 (amino acids 139 to 1033) without PYD was subcloned into a modified baculoviral vector pFastBac with an MBP

tag and a linker peptide YCAKYRA at the N terminus. The plasmids encoding NLRP3 mutants (K593R, K171R, K339R, K353R, K373R, K380R, K492R, K543R, K675R, and K820R), gRNA-resistant (r) human (h)/mouse (m) WT NLRP3, or h/mrNLRP3 K593R mutant were generated using a ClonExpress MultiS One Step Cloning Kit (Vazyme Biotech #C113). DNA fragments encoding cyanase and urease were synthesized by Genewiz and ligated into a pLVX-Tet on lentiviral vector digested with Eco RI and Age I. The sequence information of gRNA oligonucleotides and PCR primers used for molecular cloning are available in table S1.

Gene KO and generation of stable cell lines

293FT cells (1×10^6) were seeded in 60-mm dishes and cotransfected with 3 μg of lentiCRISPRv2-gRNA plasmid, 1.5 μg of pMD2.G plasmid (Addgene #12259), and 1.5 μg of psPAX2 plasmid (Addgene #12260) using Lipofectamine 2000 (Thermo Fisher Scientific). Forty-eight hours after transfection, supernatants containing lentiviruses were harvested, centrifuged at 600*g* for 10 min, and then passed through filters with a pore size of 0.45 μm. THP-1 cells and iBMDMs were infected with lentiviruses at an MOI (multiplicity of infection) of 1 in the presence of polybrene (8 μg ml^{-1}), followed by selection with puromycin (1 μg ml^{-1}) for 7 days. The KO efficiency was evaluated by immunoblotting analysis.

For rescued expression of NLRP3 in *NLRP3*/*Nlrp3*-KO THP-1 cells and iBMDMs, lentiviruses expressing FLAG-tagged gRNA-resistant (r) WT h/mrNLRP3 or h/mrNLRP3 K593R mutant were produced and used to infect target cells as mentioned above. Likewise, to construct 293T cells stably expressing mouse GSDMD, lentiviruses expressing mouse GSDMD were produced and used to infect 293T cells as mentioned above. Infected cells were cultured with a medium containing hygromycin (200 μg ml^{-1}) for 14 days, followed by immunoblotting analysis to evaluate expression of the target proteins.

Expression and purification of recombinant proteins

For expression and purification of NEK7 recombinant protein, BL21 (DE3) cells transformed with pGEX4T-1 NEK7 plasmid were inoculated in 500 ml of LB medium supplemented with ampicillin (50 μg ml^{-1}) and treated with 0.2 mM IPTG when the OD_{600} (optical density at 600 nm) of bacterial suspension reached 0.8. After culturing overnight at 16°C, the bacterial cells were harvested and resuspended in 20 ml of lysis buffer (50 mM tris-HCl, pH 7.5, 500 mM NaCl, 5 mM $MgCl_2$, 10% glycerol, 1 mM β-mercaptoethanol, and 100 μM PMSF). The lysates were sonicated for 15 min on ice followed by centrifugation at 18,000*g* for 30 min at 4°C. The supernatants were loaded onto a GSTrap HP column (GE Healthcare Life Sciences) followed by elution with 10 mM reduced glutathione. The eluted samples were desalted with a 30-kDa spin column and then further purified using a Superdex-200 size exclusion column (GE Healthcare Life Sciences).

For expression and purification of NLRP3 recombinant protein, 1 liter of Sf9 cells (3×10^6 cells ml^{-1}) were infected with baculoviruses expressing His-MBP–tagged NLRP3. Forty-eight hours after viral infection, the cells were harvested and lysed by sonication on ice in 20 ml of lysis buffer [20 mM tris-HCl, pH 7.5, 200 mM NaCl, 0.5 mM Tris (2-carboxyethyl)phosphine (TCEP), and 10% glycerol] supplemented with protease inhibitor cocktail. The lysates were centrifuged at 18,000*g* for 30 min at 4°C, and the supernatants were loaded onto an amylose resin affinity column followed by elution with 25 mM maltose solution in the lysis buffer. The sample was desalted with a 30-kDa spin column and then further purified using a Superose 6 size exclusion column (GE Healthcare Life Sciences). The purified proteins were concentrated and kept in store buffer (20 mM tris-HCl, pH 7.5, 150 mM NaCl, 0.5 mM TCEP, 10% glycerol) at −80°C for further use. To examine the efficiency of protein purification, the purified protein samples (~50 ng) were separated on 10% SDS–polyacrylamide gel electrophoresis (PAGE) and then stained with a Fast Silver staining kit (Beyotime #P0017S) following the manufacturer's instructions.

Immunoblotting and immunoprecipitation

Immunoblotting and immunoprecipitation assays were performed as described previously (*39*). For immunoblotting assay, approximately 1×10^6 cells grown in six-well plates were washed thrice with ice-cold PBS and then lysed in a modified lysis buffer (25 mM tris-HCl, pH 7.4, 0.1% SDS, 1% Triton X-100, 150 mM NaCl, 0.5 mM EDTA, 100 μM leupeptin, and complete protease inhibitor cocktail). The cell lysates were centrifuged at 13,200*g* for 15 min at 4°C. The supernatants were collected, and total protein concentration was measured using a Bicinchoninic Acid (BCA) protein assay kit (Thermo Fisher Scientific #23225). Equal amount (30 μg) of the samples was separated on 8%, 10%, or 12% SDS-PAGE and then transferred onto a 0.22-μm PVDF membrane (Millipore) by a wet transfer. The membranes were probed with specific primary antibodies and then HRP-conjugated secondary antibodies. The immunoblots were developed with SuperSignal West Pico Chemiluminescent Substrate (Thermo Fisher Scientific) and visualized using a ChemiScope 6000 Exp instrument (Clinx Science Instruments). The band intensity was quantified using the ImageJ software.

For immunoprecipitation experiment, approximately 5×10^6 cells grown in 10-cm dishes were lysed in lysis buffer [25 mM tris-HCl, pH 7.4, 0.1% SDS, 1% Triton X-100, 150 mM NaCl, 0.5 mM EDTA, 5% (v/v) glycerol, and complete protease inhibitor cocktail]. The cell lysates were centrifuged at 13,200*g* for 15 min at 4°C, and supernatants were collected. To precipitate endogenous proteins, the supernatants (2 mg/ml total protein) were incubated with specific primary antibodies (2 μg ml^{-1}) overnight followed by incubation with 25 μl of protein A/G magnetic beads (Thermo Fisher Scientific) for another 2 hours at 4°C. To precipitate tagged proteins, the supernatants (2 mg/ml total protein) were incubated with 25 μl of anti-HA nanobody magarose beads (AlpalifeBio #KTSM1335) or anti-FLAG M2 affinity gel (Sigma #A2220) for 2 hours at 4°C followed by washing thrice with lysis buffer. Immunoprecipitated protein complexes were analyzed by immunoblotting.

Depletion of K593-carbamoylated NLRP3

A total of 1×10^7 cells grown in 15-cm dishes were stimulated with LPS (100 ng ml^{-1}) for 8 hours. The cells were lysed in lysis buffer [25 mM tris-HCl, pH 7.4, 0.1% SDS, 1% Triton X-100, 150 mM NaCl, 0.5 mM EDTA, 5% (v/v) glycerol, and complete protease inhibitor cocktail] and centrifuged at 13,200*g* for 15 min at 4°C to remove the debris. One quarter of the cell lysate was incubated with normal IgG or NLRP3 K593ca primary antibodies (4 μg ml^{-1}) overnight at 4°C in the presence of NLRP3 normal peptide or NLRP3 K593ca peptide (10 μg ml^{-1}). The samples were then incubated with 25 μl of protein A/G magnetic beads (Thermo Fisher Scientific) for another 2 hours at 4°C. The supernatants, immunoprecipitants, and input cell lysates were analyzed by immunoblotting. The percentage (%) of NLRP3 depletion by immunoprecipitation with NLRP3 K593ca antibodies was quantified as the deduction of relative NLRP3 band intensity in samples immunoprecipitated with NLRP3 K593ca antibodies compared to the sample immunoprecipitated with normal IgG.

Inflammasome activation assay

Macrophages were plated at a density of 1×10^6 cells per well in 60-mm dishes 24 hours before treatment with LPS or pam3CSK4. Unless stated, the cells were primed with LPS (100 ng ml^{-1}) for 8 hours and then stimulated with 10 μM Nig for 45 min, 5 mM ATP for 45 min, or MSU crystals (300 μg ml^{-1}) for 60 min to activate the NLRP3 inflammasome. The LPS-primed cells were also transfected with 1.5 μg of poly(dA:dT) or 1.6 μg of purified flagellin using Lipofectamine 2000 (Invitrogen #11668027) to activate AIM2 inflammasome and NLRC4 inflammasome, respectively. To noncanonically activate NLRP3 inflammasome, the LPS-primed cells were electroporated with 2 μg of LPS using Neon Transfection system (Life technologies). After stimulation, supernatants and cell lysates were collected separately for further analyses. Released IL-1β and IL-18 were detected using an ELISA kit (Abcam #ab214025 and #ab100705 for human IL-1β and mouse IL-1β, respectively; Boster Biological Technology #EK0864 and #EK0433 for human IL-18 and mouse IL-18, respectively).

LDH assay

The release of LDH from pyroptotic cells was measured using a CytoTox 96 nonradioactive cytotoxicity assay kit (Promega #G1780) following the manufacturer's protocol. Briefly, cultural supernatants (50 μl) were mixed with equal volume of CytoTox 96 reagent and incubated for 30 min at room temperature in the dark. The reaction was terminated by adding 50 μl of stop solution into each well. The plates were read at absorbance of 490 nm using a BioTek microplate reader, and fresh medium served as a background absorbance.

NLRP3 inflammasome reconstitution

NLRP3 inflammasome was reconstituted as described previously (*29*). Briefly, 293T cells stably expressing mouse GSDMD were plated in six-well plates at a density of 5×10^5 per well 16 hours before transfection. The cells were cotransfected with plasmids expressing murine NLRP3 inflammasome components, including WT FLAG-NLRP3 or mutated FLAG-NLRP3 (800 ng), V5-ASC (80 ng), HA-NEK7 (800 ng), and Myc-pro-caspase-1 (400 ng), using Lipofectamine 2000. The effect of cyanate treatment on activation of reconstituted NLRP3 inflammasome was examined 24 hours after transfection.

ASC oligomerization

ASC oligomerization was detected following the procedures described previously with minor adjustments (*40*). Briefly, a total number of 1×10^6 cells grown in 60-mm dishes were washed twice with ice-cold PBS and then lysed with crosslinking lysis buffer (50 mM Hepes, 0.5% Triton X-100, 100 μM PMSF, 100 μM leupeptin, 1 mM Na_3VO_4) on ice for 20 min. The cell lysates were centrifuged at 6000*g* for 10 min at 4°C. The pellets were washed twice with 50 mM Hepes buffer, resuspended in 200 μl of crosslinking buffer (50 mM Hepes, 150 mM NaCl), and then cross-linked with 2 mM BS^3 for 1 hour at 37°C. The cross-linked samples were centrifuged at 6000*g* for 10 min at 4°C. The resulting pellets were dissolved directly in 2 × SDS sample buffer (40 μl) and then analyzed by immunoblotting.

Cell viability assay

Cells were plated at a density of 5×10^3 cells per well in 96-well plate 24 hours before cyanate treatment. The cells were treated with 0.5 or 1 mM cyanate for 30 min, washed twice with PBS, and cultured for another 12 hours. Cell viability was measured using a luminescent cell viability assay kit (Promega #G7570) following the manufacturer's protocol. Briefly, 100 μl of CellTiter-Glo regent was added into each well, and then the samples were incubated for 10 min at room temperature to lyse the cells. Luminescence signal was measured using a multifunction BioTek microplate reader. Fresh medium served as a background absorbance.

Cell fractionation

Cell fractionation was performed according to the previous publication with minor modifications (*32*). Two dishes of cells (~1×10^7 cells per 15-cm dish) were treated with LPS (100 ng ml^{-1}) for 8 hours and then stimulated with 10 μM Nig for 45 min. The cells in each dish were washed twice with ice-cold PBS and homogenized in 500 μl of ice-cold isotonic buffer (0.25 M sucrose, 10 mM tris-HCl, pH 7.5, 10 mM KCl, 1.5 mM $MgCl_2$, and protease inhibitor cocktail). Cell lysates from the same treatments were combined and centrifuged at 1000*g* for 5 min at 4°C to remove nucleus pellet (P1). The resulting supernatant (S1) was centrifuged at 5000*g* for 10 min at 4°C to obtain heavy membrane fraction (pellet, P5), and then this supernatant (S5) was further centrifuged at 100,000*g* at 4°C for 20 min to obtain the light membrane fraction (pellet, P100) and the cytosol fraction (supernatant, S100). The fraction P5 and P100 were harvested, washed once with isotonic buffer, resuspended in 100 μl of lysis buffer (25 mM tris-HCl, pH 7.4, 0.1% SDS, 1% Triton X-100, 150 mM NaCl, 0.5 mM EDTA, 100 μM leupeptin, and protease inhibitor cocktail), and analyzed by immunoblotting.

RNA extraction and qPCR

RNA extraction and qPCR analysis were performed as described previously with minor adjustments (*39*). Briefly, total RNA was extracted by the TRIzol regent (Invitrogen) and then reversely transcribed to complementary DNA (cDNA) in a 20-μl reaction using a PrimeScript RT Reagent Kit (Takara Bio #RR037A). cDNA was amplified with a PerfectStart Green qPCR Super Mix kit (TransGen Biotech #AQ602), and qPCR was performed using an ABI Q7 Fast Real Time PCR System (Applied Biosystems) following the manufacturer's protocol. *ACTB*/*Actb* served as a housekeeping gene. ΔC_t of a sample was obtained by subtracting the C_t of the target gene from the C_t of *ACTB*/*Actb*. Relative expression levels of target genes in each sample were calculated as $2^{\Delta Ct}$. The sequences of primers used for qPCR were listed in table S1.

Dot blot assay

Synthetic peptides (1 mg) were dissolved in 1 ml of ultrapure water and serially diluted to different concentrations (200, 20, and 2 ng ml^{-1}). Equal volume (1 μl) of each sample was spotted on nitrocellulose membranes, dried for 1 hour, and then blocked with 5% nonfat milk for 1 hour at room temperature. Following blocking, the membranes were probed with primary antibodies (1 μg ml^{-1}) recognizing NLRP3 K593ca overnight at 4°C and then incubated with the HRP-conjugated anti-rabbit antibody for 1 hour at room temperature. Immunoblots were visualized using a ChemiScope 6000 Exp instrument (Clinx Science Instruments) following development with the SuperSignal West Pico Chemiluminescent Substrate (Thermo Fisher Scientific).

Flow cytometry

Flow cytometry was performed as described previously with minor adjustments (*39*). To analyze the purity of primary murine macrophages, approximately 1×10^6 isolated mBMDMs grown in 60-mm dishes were harvested by cell scraper and washed twice with ice-cold PBS. The cells were then stained with APC anti-mouse F4/80 and FITC anti-mouse CD11b (1 μg ml^{-1}) for 30 min at 4°C. The cells were washed twice with ice-cold PBS, transferred to FACS (fluorescence-activated cell sorting) tubes, and then loaded onto a BD LSRFortessa flow cytometer with gating to exclude debris and doublets. A total of 20,000 cells per sample were analyzed using the FlowJo software.

In vitro carbamoylation assay

To test the isocyanic acid–mediated NLRP3 K593ca, purified WT His-MBP-NLRP3 or His-MBP-NLRP3 K593R protein (200 ng) was incubated with 1 mM cyanate for 1 hour at 37°C in 25 μl of reaction buffer (25 mM tris-HCl, pH 8.0, 150 mM NaCl, 100 μM PMSF, 100 μM leupeptin).

GST pull-down assay

Purified WT His-MBP-NLRP3 or His-MBP-NLRP3 K593R protein (400 ng per sample) was incubated with 1 mM cyanate for 1 hour at 37°C in 50 μl of reaction buffer (25 mM tris-HCl, pH 8.0, 150 mM NaCl, 100 μM PMSF, 100 μM leupeptin). The samples were then incubated with agarose bead–immobilized GST-NEK7 protein (200 ng) for 2 hours at room temperature, followed by washing thrice with a modified binding buffer (25 mM tris-HCl, pH 8.0, 150 mM NaCl, 1% Triton X-100, 100 μM PMSF, 100 μM leupeptin). The immobilized proteins were denatured by boiling in 5 × SDS sample buffer (50 μl) for 10 min and then analyzed by immunoblotting.

MS analysis of lysine carbamoylation on NLRP3

iBMDMs without or with FLAG-NLRP3 expression were treated with ^{15}N-labeled cyanate (1 mM) for 1 hour. Immunoprecipitated FLAG-NLRP3 sample was separated using SDS-PAGE followed by staining with Coomassie brilliant blue. The band corresponding to FLAG-NLRP3 was excised and digested with trypsin overnight. Digested sample was analyzed on a nanoLC Q-Exactive mass spectrometer (Thermo Fisher Scientific) in line with an Easy-nLC 1000 HPLC system (Thermo Fisher). MS/MS spectra from each LC-MS/MS run were searched against the mouse NLRP3 sequence using the Proteome Discoverer (Thermo Fischer Scientific version 1.4.0.288) searching algorithm with the following criteria: Full tryptic specificity was required, two missed cleavages were allowed, precursor ion mass tolerance was set to 10 ppm, fragment ion mass tolerance was 0.02 Da, and peptide FDR (false discovery rate) was set to 1%. Oxidation (M) and homocitrulline (K +44.013 Da) were set as variable modifications.

Sample extraction for LC-MS

A total number of 1×10^7 cells seeded in 10-cm dishes were washed twice with ice-cold PBS, and then 1 ml of extraction solution composed of methanol and water (8: 2) was added to each dish. The cell lysates were harvested using a cell scraper and vortexed at 1000 rpm for 10 min at 4°C, followed by centrifugation at 15,000*g* for 20 min at 4°C. The collected supernatant (980 μl) was dried by vacuum evaporation using a refrigerated CentriVap Concentrator (Labconco) and then reconstituted in optimized volumes (25 μl for isocyanic acid; 200 μl for citrulline, ornithine, and urea) of methanol.

Isocyanic acid derivatization and measurement with LC-MS

To measure isocyanic acid concentration, a carbamoylation assay was performed as described previously (*41*) with minor modification. Briefly, the extraction sample (25 μl) was incubated with 1.5 μl of 1 M acetic acid and 1.5 μl of 1 M 2-aminobenzoic acid for 30 min at 42°C water bath. The mixture was then acidified by addition of 2 μl of 12 N HCl, followed by centrifugation at 13,000*g* for 10 min at 4°C, and 10 μl of the supernatant was analyzed by a Ultra-performance liquid chromatography coupled with quadrupole time of flight mass spectrometry (UPLC-QTOF-MS) column (Phenomenex Kinetex #00D-4462-AN). The mobile phase was 0.1% formic acid in water (A) and 0.1% formic acid in acetonitrile (B). Samples were injected into the column and separated at a flow rate of 0.2 ml min^{-1}. Buffer gradient was set as follows: 98% A and 2% B during 0 to 2 min, 10% A and 90% B during 2 to 7 min, 98% A and 2% B during 7 to 10 min. LC-MS was performed on a 6530 Liquid Chromatography/Quadrupole-TOF mass spectrometer (Agilent) operated in positive mode. The end product of derivatization (2,4-quinazolinedione) was monitored at mass/charge ratio (*m*/*z*) 163.05. The amount of isocyanic acid in each sample was calculated according to the standard curve generated by serial concentrations of 2,4-quinazolinedione and then normalized to the cell number.

Intracellular metabolite profiling with LC-MS

To measure citrulline, ornithine, and urea concentrations, the samples were separated by an ACQUITY UPLC BEH HILIC column (1.7 μm, 2.1 mm × 100 mm; Waters #186003461) with a mobile phase composed of solution A (10 mM ammonium acetate in water) and solution B (100% acetonitrile). A total volume of 10 μl of sample was injected into the column and separated at a flow rate of 0.3 ml min^{-1} at 40°C. Buffer gradient was set as follows: 2% A and 98% B during 0 to 1.5 min, 98% A and 2% B during 1.5 to 8 min, 2% A and 98% B during 8 to 20 min for ornithine; 10% A and 90% B during 0 to 1.5 min, 98% A and 2% B during 1.5 to 7 min, 10% A and 90% B during 7 to 11 min for citrulline; 2% A and 98% B during 0 to 1.5 min, 98% A and 2% B during 1.5 to 10 min, 2% A and 98% B during 10 to 15 min for urea. The amount of citrulline, ornithine, and urea in each sample was calculated according to the standard curve generated by serial concentrations of the corresponding metabolites and then normalized to the cell number.

^{13}C-isotope labeling study

Macrophages were plated at a density of 1×10^6 cells per well in 60-mm dishes in phenol red–free DMEM (Gibco #21063029) supplemented with 10% FBS and 2 mM ureido-^{13}C-citrulline (Cambridge Isotope Laboratories #CLM-4899-PK). Twenty-four hours later, the medium was replaced with fresh medium, followed by treatment of the cells with LPS for 8 hours. Cells were washed twice with 10 ml of ice-cold PBS and then extracted with 1 ml of extraction solution composed of methanol and water (8: 2). The cell lysates were harvested using a cell scraper and centrifuged at 15,000*g* for 20 min at 4°C. The collected supernatant (980 μl) was dried by vacuum evaporation using a refrigerated CentriVap Concentrator (Labconco), followed by resuspension in 25 μl of methanol. To detect ^{13}C-labeled isocyanic acid, the extraction sample (25 μl) was derivatized with 1.5 μl of 1 M acetic acid and 1.5 μl of 1 M 2-aminobenzoic acid for 30 min at 42°C water bath, and then acidified by addition of 2 μl of 12 N HCl. Aliquoted sample (10 μl) was loaded onto a UPLC-QTOF-MS column (Phenomenex Kinetex #00D-4462-AN) and separated at a flow rate of 0.2 ml min^{-1} with buffer (A: 0.1% formic acid in water; B: 0.1% formic acid in acetonitrile) gradient as follows: 98% A and 2% B during 0 to 2 min, 10% A and 90% B during 2 to 7 min, 98% A and 2% B during 7 to 10 min. LC-MS was performed on a 6530 Liquid Chromatography/Quadrupole-TOF mass spectrometer (Agilent) operated in positive mode. The end product of derivatization (^{13}C-labeled 2,4-quinazolinedione) was monitored at *m*/*z* 164.05.

Statistical analysis

Statistical analyses were performed using the IBM SPSS Statistics 23 or GraphPad Prism 8.0.2. All immunoblotting experiments were independently repeated at least three times and presented as a representative example of a single experiment. Sample numbers and experimental repeats are described in figure legends. Quantitative data are presented as mean ± SD or mean ± SEM. Two-tailed Student's *t* test was used for comparison of paired variables, and one-way analysis of variance (ANOVA) was used for comparison of multiple variables. Survival curves were compared using the two-tailed log-rank test. Clinical

scores for sepsis severity of mice were compared using the linear mixed model. *P* values less than 0.05 were considered statistically significant.

Supplementary Materials

The PDF file includes:
Figs. S1 to S8
Table S1
Legend for data S1
Data S2

Other Supplementary Material for this manuscript includes the following:
Data S1

REFERENCES AND NOTES

1. M. Lamkanfi, V. M. Dixit, Mechanisms and functions of inflammasomes. *Cell* **157**, 1013–1022 (2014).
2. P. Broz, V. M. Dixit, Inflammasomes: Mechanism of assembly, regulation and signalling. *Nat. Rev. Immunol.* **16**, 407–420 (2016).
3. K. V. Swanson, M. Deng, J. P. Ting, The NLRP3 inflammasome: Molecular activation and regulation to therapeutics. *Nat. Rev. Immunol.* **19**, 477–489 (2019).
4. H. Sharif, L. Wang, W. L. Wang, V. G. Magupalli, L. Andreeva, Q. Qiao, A. V. Hauenstein, Z. Wu, G. Nunez, Y. Mao, H. Wu, Structural mechanism for NEK7-licensed activation of NLRP3 inflammasome. *Nature* **570**, 338–343 (2019).
5. X. Liu, Z. Zhang, J. Ruan, Y. Pan, V. G. Magupalli, H. Wu, J. Lieberman, Inflammasome-activated gasdermin D causes pyroptosis by forming membrane pores. *Nature* **535**, 153–158 (2016).
6. J. Shi, W. Gao, F. Shao, Pyroptosis: Gasdermin-mediated programmed necrotic cell death. *Trends Biochem. Sci.* **42**, 245–254 (2017).
7. N. Kayagaki, O. S. Kornfeld, B. L. Lee, I. B. Stowe, K. O'Rourke, Q. Li, W. Sandoval, D. Yan, J. Kang, M. Xu, J. Zhang, W. P. Lee, B. S. McKenzie, G. Ulas, J. Payandeh, M. Roose-Girma, Z. Modrusan, R. Reja, M. Sagolla, J. D. Webster, V. Cho, T. D. Andrews, L. X. Morris, L. A. Miosge, C. C. Goodnow, E. M. Bertram, V. M. Dixit, NINJ1 mediates plasma membrane rupture during lytic cell death. *Nature* **591**, 131–136 (2021).
8. M. Degen, J. C. Santos, K. Pluhackova, G. Cebrero, S. Ramos, G. Jankevicius, E. Hartenian, U. Guillerm, S. A. Mari, B. Kohl, D. J. Muller, P. Schanda, T. Maier, C. Perez, C. Sieben, P. Broz, S. Hiller, Structural basis of NINJ1-mediated plasma membrane rupture in cell death. *Nature* **618**, 1065–1071 (2023).
9. L. David, J. P. Borges, L. R. Hollingsworth, A. Volchuk, I. Jansen, E. Garlick, B. E. Steinberg, H. Wu, NINJ1 mediates plasma membrane rupture by cutting and releasing membrane disks. *Cell* **187**, 2224–2235.e16 (2024).
10. S. Ramos, E. Hartenian, P. Broz, Programmed cell death: NINJ1 and mechanisms of plasma membrane rupture. *Trends Biochem. Sci.* **49**, 717–728 (2024).
11. C. Skon-Hegg, J. Zhang, X. Wu, M. Sagolla, N. Ota, A. Wuster, J. Tom, E. Doran, N. Ramamoorthi, P. Caplazi, J. Monroe, W. P. Lee, T. W. Behrens, LACC1 regulates TNF and IL-17 in mouse models of arthritis and inflammation. *J. Immunol.* **202**, 183–193 (2019).
12. J. W. Kang, J. Yan, K. Ranjan, X. Zhang, J. R. Turner, C. Abraham, Myeloid cell expression of LACC1 is required for bacterial clearance and control of intestinal inflammation. *Gastroenterology* **159**, 1051–1067 (2020).
13. M. Z. Cader, K. Boroviak, Q. Zhang, G. Assadi, S. L. Kempster, G. W. Sewell, S. Saveljeva, J. W. Ashcroft, S. Clare, S. Mukhopadhyay, K. P. Brown, M. Tschurtschenthaler, T. Raine, B. Doe, E. R. Chilvers, J. L. Griffin, N. C. Kaneider, R. A. Floto, M. D'Amato, A. Bradley, M. J. Wakelam, G. Dougan, A. Kaser, C13orf31 (FAMIN) is a central regulator of immunometabolic function. *Nat. Immunol.* **17**, 1046–1056 (2016).
14. O. Omarjee, A. L. Mathieu, G. Quiniou, M. Moreews, M. Ainouze, C. Frachette, I. Melki, C. Dumaine, M. Gerfaud-Valentin, A. Duquesne, T. Kallinich, E. Tahir Turanli, C. Malcus, S. Viel, R. Pescarmona, S. Georgin-Lavialle, Y. Jamilloux, J. P. Larbre, G. Sarrabay, F. Magnotti, G. I. Rice, F. Bleicher, J. Reboulet, S. Merabet, T. Henry, Y. J. Crow, M. Faure, T. Walzer, A. Belot, LACC1 deficiency links juvenile arthritis with autophagy and metabolism in macrophages. *J. Exp. Med.* **218**, e20201006 (2021).
15. M. Z. Cader, R. P. de Almeida Rodrigues, J. A. West, G. W. Sewell, M. N. Md-Ibrahim, S. Reikine, G. Sirago, L. W. Unger, A. B. Iglesias-Romero, K. Ramshorn, L. M. Haag, S. Saveljeva, J. F. Ebel, P. Rosenstiel, N. C. Kaneider, J. C. Lee, T. D. Lawley, A. Bradley, G. Dougan, Y. Modis, J. L. Griffin, A. Kaser, FAMIN is a multifunctional purine enzyme enabling the purine nucleotide cycle. *Cell* **180**, 278–295.e23 (2020).
16. S. Saveljeva, G. W. Sewell, K. Ramshorn, M. Z. Cader, J. A. West, S. Clare, L. M. Haag, R. P. de Almeida Rodrigues, L. W. Unger, A. B. Iglesias-Romero, L. M. Holland, C. Bourges, M. N. Md-Ibrahim, J. O. Jones, R. S. Blumberg, J. C. Lee, N. C. Kaneider, T. D. Lawley, A. Bradley, G. Dougan, A. Kaser, A purine metabolic checkpoint that prevents autoimmunity and autoinflammation. *Cell Metab.* **34**, 106–124.e10 (2022).
17. Z. Wei, J. Oh, R. A. Flavell, J. M. Crawford, LACC1 bridges NOS2 and polyamine metabolism in inflammatory macrophages. *Nature* **609**, 348–353 (2022).
18. S. Delanghe, J. R. Delanghe, R. Speeckaert, W. Van Biesen, M. M. Speeckaert, Mechanisms and consequences of carbamoylation. *Nat. Rev. Nephrol.* **13**, 580–593 (2017).
19. Z. Wang, S. J. Nicholls, E. R. Rodriguez, O. Kummu, S. Horkko, J. Barnard, W. F. Reynolds, E. J. Topol, J. A. DiDonato, S. L. Hazen, Protein carbamylation links inflammation, smoking, uremia and atherogenesis. *Nat. Med.* **13**, 1176–1184 (2007).
20. D. El-Gamal, S. P. Rao, M. Holzer, S. Hallstrom, J. Haybaeck, M. Gauster, C. Wadsack, A. Kozina, S. Frank, R. Schicho, R. Schuligoi, A. Heinemann, G. Marsche, The urea decomposition product cyanate promotes endothelial dysfunction. *Kidney Int.* **86**, 923–931 (2014).
21. C. L. Hawkins, Role of cyanate in the induction of vascular dysfunction during uremia: More than protein carbamylation? *Kidney Int.* **86**, 875–877 (2014).
22. S. Jaisson, C. Pietrement, P. Gillery, Carbamylation-derived products: Bioactive compounds and potential biomarkers in chronic renal failure and atherosclerosis. *Clin. Chem.* **57**, 1499–1505 (2011).
23. N. A. Schmacke, F. O'Duill, M. M. Gaidt, I. Szymanska, J. M. Kamper, J. L. Schmid-Burgk, S. C. Madler, T. Mackens-Kiani, T. Kozaki, D. Chauhan, D. Nagl, C. A. Stafford, H. Harz, A. L. Frohlich, F. Pinci, F. Ginhoux, R. Beckmann, M. Mann, H. Leonhardt, V. Hornung, IKKβ primes inflammasome formation by recruiting NLRP3 to the trans-Golgi network. *Immunity* **55**, 2271–2284.e7 (2022).
24. V. A. K. Rathinam, Y. Zhao, F. Shao, Innate immunity to intracellular LPS. *Nat. Immunol.* **20**, 527–533 (2019).
25. K. Engel, W. Hohne, J. Haberle, Mutations and polymorphisms in the human argininosuccinate synthetase (ASS1) gene. *Hum. Mutat.* **30**, 300–307 (2009).
26. N. A. Kamennaya, A. F. Post, Characterization of cyanate metabolism in marine Synechococcus and Prochlorococcus spp. *Appl. Environ. Microbiol.* **77**, 291–301 (2011).
27. H. L. Mobley, M. D. Island, R. P. Hausinger, Molecular biology of microbial ureases. *Microbiol. Rev.* **59**, 451–480 (1995).
28. J. Shi, Y. Zhao, K. Wang, X. Shi, Y. Wang, H. Huang, Y. Zhuang, T. Cai, F. Wang, F. Shao, Cleavage of GSDMD by inflammatory caspases determines pyroptotic cell death. *Nature* **526**, 660–665 (2015).
29. H. Shi, A. Murray, B. Beutler, Reconstruction of the mouse inflammasome system in HEK293T cells. *Bio. Protoc.* **6**, e1986 (2016).
30. T. Kallinich, A. Thorwarth, S. L. von Stuckrad, A. Rosen-Wolff, H. Luksch, P. Hundsdoerfer, K. Minden, P. Krawitz, Juvenile arthritis caused by a novel FAMIN (LACC1) mutation in two children with systemic and extended oligoarticular course. *Pediatr. Rheumatol. Online J.* **14**, 63 (2016).
31. A. Singh, D. Suri, P. Vignesh, G. Anjani, P. Jacob, K. M. Girisha, LACC1 gene mutation in three sisters with polyarthritis without systemic features. *Ann. Rheum. Dis.* **79**, 425–426 (2020).
32. J. Chen, Z. J. Chen, PtdIns4P on dispersed trans-Golgi network mediates NLRP3 inflammasome activation. *Nature* **564**, 71–76 (2018).
33. N. Song, Z. S. Liu, W. Xue, Z. F. Bai, Q. Y. Wang, J. Dai, X. Liu, Y. J. Huang, H. Cai, X. Y. Zhan, Q. Y. Han, H. Wang, Y. Chen, H. Y. Li, A. L. Li, X. M. Zhang, T. Zhou, T. Li, NLRP3 phosphorylation is an essential priming event for inflammasome activation. *Mol. Cell* **68**, 185–197.e6 (2017).
34. M. S. J. Mangan, E. J. Olhava, W. R. Roush, H. M. Seidel, G. D. Glick, E. Latz, Targeting the NLRP3 inflammasome in inflammatory diseases. *Nat. Rev. Drug Discov.* **17**, 588–606 (2018).
35. A. Hooftman, S. Angiari, S. Hester, S. E. Corcoran, M. C. Runtsch, C. Ling, M. C. Ruzek, P. F. Slivka, A. F. McGettrick, K. Banahan, M. M. Hughes, A. D. Irvine, R. Fischer, L. A. J. O'Neill, The immunomodulatory metabolite itaconate modifies NLRP3 and inhibits inflammasome activation. *Cell Metab.* **32**, 468–478.e7 (2020).
36. P. Dirnhuber, F. Schutz, The isomeric transformation of urea into ammonium cyanate in aqueous solutions. *Biochem. J.* **42**, 628–632 (1948).
37. M. Holzer, K. Zangger, D. El-Gamal, V. Binder, S. Curcic, V. Konya, R. Schuligoi, A. Heinemann, G. Marsche, Myeloperoxidase-derived chlorinating species induce protein carbamylation through decomposition of thiocyanate and urea: Novel pathways generating dysfunctional high-density lipoprotein. *Antioxid. Redox Signal.* **17**, 1043–1052 (2012).
38. M. Bougaki, R. J. Searles, K. Kida, J. Yu, E. S. Buys, F. Ichinose, Nos3 protects against systemic inflammation and myocardial dysfunction in murine polymicrobial sepsis. *Shock* **34**, 281–290 (2010).
39. Z. Zhang, C. Chen, F. Yang, Y. X. Zeng, P. Sun, P. Liu, X. Li, Itaconate is a lysosomal inducer that promotes antibacterial innate immunity. *Mol. Cell* **82**, 2844–2857.e10 (2022).
40. D. Wang, Y. Zhang, X. Xu, J. Wu, Y. Peng, J. Li, R. Luo, L. Huang, L. Liu, S. Yu, N. Zhang, B. Lu, K. Zhao, YAP promotes the activation of NLRP3 inflammasome via blocking K27-linked polyubiquitination of NLRP3. *Nat. Commun.* **12**, 2674 (2021).
41. P. Lundquist, B. Backman-Gullers, B. Kagedal, L. Nilsson, H. Rosling, Fluorometric determination of cyanate in plasma by conversion to 2,4(1H,3H)-quinazolinedione and

separation by high-performance liquid chromatography. *Anal. Biochem.* **211**, 23–27 (1993).

Acknowledgments: We thank F. Shao (NIBS) for providing iBMDM cell line. We thank Z. Xie and X. Ding (Core Facility of Protein Sciences, Institute of Biophysics) for MS technical assistances. **Funding:** This work was supported by the National Key R&D Program of China (grant no. 2024YFA1307400 to X.L.), the Training Program of the Major Research Plan of the National Natural Science Foundation of China (grant no. 92157104 to X.L.), the National Natural Science Foundation of China (grant no. 82073060 to X.L. and grant no. 82371786 to Z.Z.), the Young Scientists Fund of the National Natural Science Foundation of China (grant no. 82103349 to C.C.), the Fund of the Youth Innovation Promotion Association of Chinese Academy of Sciences (2023103 to Z.Z.), and the Fund of the State Key Laboratory of Epigenetic Regulation and Intervention, CAS (grant no. O4CCSGZ301 to X.L.). **Author contributions:** Conceptualization: Z.Z. and X.L. Methodology: X.L. Validation: Z.Z., C.C., and X.L. Investigation: Z.Z., C.C., C.L., P.S., P.L., S.F., and X.L. Resources: Z.Z., C.C., C.L., P.L., and S.F. Data curation: Z.Z. and C.C. Formal analysis: Z.Z., C.L., and P.L. Visualization: Z.Z. and X.L. Supervision: X.L. Writing—original draft: Z.Z. and X.L. Writing—review and editing: Z.Z., C.C., C.L., P.L., S.F., and X.L. Project administration: Z.Z., C.C., P.L., and X.L. Funding acquisition: Z.Z., C.C., and X.L. **Competing interests:** The authors declare that they have no competing interests. **Data and materials availability:** All data needed to evaluate the conclusions in the paper are present in the paper and/or the Supplementary Materials.

Submitted 13 May 2024
Accepted 29 January 2025
Published 7 March 2025
10.1126/sciadv.adq4266